Comenius University in Bratislava
Faculty of Mathematics, Physics and Informatics

Testing Independence of Compte's Spatial Working Memory Model from the Neuron Model

Master's Thesis

2020
Bc. Adam Štefunko

Comenius University in Bratislava
Faculty of Mathematics, Physics and Informatics

Testing Independence of Compte's Spatial Working Memory Model from the Neuron Model

Master's Thesis

Study Programme:	Cognitive Science
Field of Study:	Computer Science
Department:	Department of Applied Informatics
Supervisor:	prof. RNDr. Ľubica Beňušková, PhD.

Bratislava, 2020
Bc. Adam Štefunko

Comenius University in Bratislava
Faculty of Mathematics, Physics and Informatics

THESIS ASSIGNMENT

Name and Surname:	Bc. Adam Štefunko
Study programme:	Cognitive Science (Single degree study, master II. deg., full time form)
Field of Study:	Computer Science
Type of Thesis:	Diploma Thesis
Language of Thesis:	English
Secondary language:	Slovak

Title: Testing Independence of Compte's Spatial Working Memory Model from the Neuron Model

Annotation: The motivation behind this work concerns the implementation level of the spatial working memory model proposed by Compte et al. (2000) who used leaky integrate-and-fire neuron model. The purpose is to verify the usability of a newer, simple model of a spiking neuron, in the oculomotor delayed-response task.

Aim: 1. Implement the spatial working memory model (Compte et al., 2000) using a simple model of spiking neurons (Izhikevich, 2003). 2. Model the delayed-response task and test independence of this model from the given neuron model.

Literature:
Compte, A., Brunel, N., Goldman-Rakic, P. S., & Wang, X. J. (2000). Synaptic mechanisms and network dynamics underlying spatial working memory in a cortical network model. Cerebral Cortex, 10(9), 910-923.
Funahashi, S., Bruce, C. J., & Goldman-Rakic, P. S. (1989). Mnemonic coding of visual space in the monkey's dorsolateral prefrontal cortex. Journal of Neurophysiology, 61(2), 331-349.
Izhikevich, E. M. (2003). Simple model of spiking neurons. IEEE Transactions on Neural Networks, 14(6), 1569-1572.

Supervisor:	prof. RNDr. Ľubica Beňušková, PhD.
Department:	FMFI.KAI - Department of Applied Informatics
Head of department:	prof. Ing. Igor Farkaš, Dr.
Assigned:	20.02.2020
Approved:	25.02.2020

prof. Ing. Igor Farkaš, Dr.
Guarantor of Study Programme

Student

Supervisor

Univerzita Komenského v Bratislave
Fakulta matematiky, fyziky a informatiky

ZADANIE ZÁVEREČNEJ PRÁCE

Meno a priezvisko študenta: Bc. Adam Štefunko
Študijný program: kognitívna veda (Jednoodborové štúdium, magisterský II. st., denná forma)
Študijný odbor: informatika
Typ záverečnej práce: diplomová
Jazyk záverečnej práce: anglický
Sekundárny jazyk: slovenský

Názov: Testing Independence of Compte's Spatial Working Memory Model from the Neuron Model
Testovanie nezávislosti Compteho modelu priestorovej pracovnej pamäti od použitého modelu neurónu

Anotácia: Motivácia pre túto prácu sa týka implementačnej úrovne modelu priestorovej pracovnej pamäti Compteho a spol. (2000) ktorí použili model deravého integrujúceho neurónu. Účelom je verifikovať použiteľnosť novšieho, jednoduchého modelu pulzného neurónu v úlohe oneskorenej okulomotorickej odpovede.

Cieľ: Compte, A., Brunel, N., Goldman-Rakic, P. S., & Wang, X. J. (2000). Synaptic mechanisms and network dynamics underlying spatial working memory in a cortical network model. Cerebral Cortex, 10(9), 910-923.
Funahashi, S., Bruce, C. J., & Goldman-Rakic, P. S. (1989). Mnemonic coding of visual space in the monkey's dorsolateral prefrontal cortex. Journal of Neurophysiology, 61(2), 331-349.
Izhikevich, E. M. (2003). Simple model of spiking neurons. IEEE Transactions on Neural Networks, 14(6), 1569-1572.

Literatúra: Compte, A., Brunel, N., Goldman-Rakic, P. S., & Wang, X. J. (2000). Synaptic mechanisms and network dynamics underlying spatial working memory in a cortical network model. Cerebral cortex, 10(9), 910-923.
Funahashi, S., Bruce, C. J., & Goldman-Rakic, P. S. (1989). Mnemonic coding of visual space in the monkey's dorsolateral prefrontal cortex. Journal of neurophysiology, 61(2), 331-349.
Izhikevich, E. M. (2003). Simple model of spiking neurons. IEEE Transactions on neural networks, 14(6), 1569-1572.

Vedúci: prof. RNDr. Ľubica Beňušková, PhD.
Katedra: FMFI.KAI - Katedra aplikovanej informatiky
Vedúci katedry: prof. Ing. Igor Farkaš, Dr.

Dátum zadania: 20.02.2020

Dátum schválenia: 25.02.2020

prof. Ing. Igor Farkaš, Dr.
garant študijného programu

Acknowledgments: I would like to thank my supervisor prof. RNDr. Ľubica Beňušková, PhD. for helping and sharing with me her knowledge about computational cognitive neuroscience, prof. Grega Repovš, PhD. for introducing me to the topic of my thesis. I especially appreciate the help and support of RNDr. Kristína Malinovská, PhD. in the final stages of writing my thesis. I also express my gratitude to Mgr. Nicole Vella for reading through my thesis and giving me feedback.

Abstract

Spatial working memory, the ability to memorize locations for a short period of time, has been studied for decades. Compte and his colleagues proposed a model of the spatial working memory used to simulate an oculomotor delayed-response task. The model consisted of excitatory pyramidal cells and inhibitory interneurons. Pyramidal cells were spatially distributed according to their sensitivity to different peripheral cue angles. Pyramidal cells closer to each other had stronger synaptic connections than those farther apart. The oculomotor delayed-response task was simulated as stimulation of pyramidal cells with a selective transient current. Pyramidal cells whose preferred angle was close to the presented cue angle exhibited elevated spiking activity which persisted after the disappearance of the stimulus. Leaky integrate-and-fire neurons were employed in the model. We implemented the model using the Simple model of spiking neurons described by Izhikevich and tested how this model behaves when different model parameters are manipulated. We showed patterns appearing in the region where neurons with preferred cue angle close to the presented cue angle resided. Although these patterns were not completely identical with findings of Compte and his colleagues, they represented a prominent and distinct manifestation of the spatially tuned stimulation of the neurons during the cue presentation. Therefore, we managed to simulate the oculomotor delayed-response task using the Simple model of spiking neurons. Results of our thesis may be used in replicating existing computational studies related to this task using the simple spiking neurons and integrating the task and the spatial working memory model to the simple spiking neurons related research.

Keywords: simple model of spiking neurons, spatial working memory, synaptic connection

Abstrakt

Priestorová pracovná pamäť, zodpovedná za krátkodobé zapamätanie si polohy v priestore, je skúmaná už desaťročia. Model priestorovej pracovnej pamäte, navrhnutý Comptem a kolektívom, bol použitý na simulovanie úlohy oneskorenej okulomotorickej reakcie. Model pozostával z excitačných pyramidálnych buniek a inhibičných interneurónov, pričom pyramidálne bunky boli priestorovo usporiadané na základe ich citlivosti na rozličné obvodové uhly. Navzájom si bližšie pyramidálne bunky mali silnejšie synaptické spojenia ako navzájom vzdialenejšie pyramidálne bunky. Úloha oneskorenej okulomotorickej reakcie bola simulovaná cez stimuláciu buniek externým dočasným prúdom, pričom čím bol obvodový uhol bunky bližšie k stimulovanému obvodovému uhlu, tým silnejším prúd bola bunka stimulovaná. Bunky dostatočne blízko k stimulovanému uhlu si vybudovali zvýšenú vzruchovú aktivitu, ktorá pretrvávala aj po skončení stimulácie. Pôvodne bol model implementovaný pomocou deravého integrujúceho neurónu. My sme implementovali model pomocou jednoduchého modelu pulzného neurónu, ktorý navrhol Izhikevich. Testovali sme, ako sa takto implementovaný model správa pri rôznych kombináciách parametrov. Objavili sme vzorce vzruchovej aktivity, ktoré sa po stimulácii objavia u neurónov dostatočne blízko k stimulovanému obvodovému uhlu. Hoci tieto vzorce neboli úplne identické s výsledkami predošlej štúdie Compteho a jeho kolegov, znamenajú výraznú a zreteľnú stopu po stimulácii neurónov. Podarilo sa nám teda nasimulovať úlohu oneskorenej okulomotorickej reakcie s použitím jednoduchého modelu pulzného neurónu. Výsledky našej práce môžu byť použité na replikáciu existujúcich výpočtových štúdií súvisiacich s úlohou oneskorenej okulomotorickej reakcie a na integráciu tejto úlohy a modelu priestorovej pracovnej pamäte do širšieho spektra výskumu používajúceho jednoduchý model pulzného neurónu.

Kľúčové slová: jednoduchý model pulzného neurónu, priestorová pracovná pamäť, synaptické spojenie

Contents

List of Figures

List of Tables

Introduction

Working memory is a phenomenon largely studied by many disciplines encompassed by cognitive science. Spatial working memory, a part of the working memory related to memorizing locations in space, has been subject to research of Funahashi et al. [10], Goldman-Rakic [12], Rao and his collective [19], and last but not least Almeida, Compte, Edin and their colleagues [1, 6, 7].

Following neuroscientific experiments with the oculomotor delayed-response task of Funahashi and his colleagues [10] and the theoretical work of Goldman-Rakic [12], Compte and his colleagues developed a computational model of the spatial working memory. This model was based on spatial tuning of synaptic connections of excitatory pyramidal cells. Each pyramidal cell coded a particular peripheral location described by its peripheral angle called the *preferred cue angle*. The closer preferred cue angles of two pyramidal cells were, the stronger their connection was. Pyramidal cells in the network received their external stimulation current based on proximity of their preferred cue angle to the peripheral angle of the location presented in the experiment. Pyramidal cells with their preferred cue close to the presented cue angle developed elevated firing activity during the stimulation. This elevated activity persisted even when the stimulation ended and was suppressed by a strong stimulation of all the neurons in the network. Detailed information on the theoretical background of our thesis can be found in chapter 1.

The model of spatial working memory [1, 6, 7] used leaky integrate-and-fire neurons, a neuron model which can simulate only a limited number of neuronal types in the human brain [15, 17]. Therefore, we implemented the model of spatial working memory [1, 6, 7] using the Simple model of spiking neurons [14], which can simulate the vast majority of cortical neurons [14, 15, 17]. Implementation details are presented in chapter 3.

We tuned several parameters of the model [1, 6, 7] in order to learn how it behaves when the Simple model of spiking neurons [14] is used. This can be seen in numerous simulations presented in chapter 4 of this thesis.

We compared the results of our simulations with the results of Compte and his colleagues [6]. Results of our simulations and their evaluation can be found in chapter 5 and section 6.1.

Chapter 1

Theoretical background

In this chapter, we present the theoretical background of our thesis. Firstly, we introduce the concept of spatial working memory and oculomotor delayed-response task. It is followed by essential mathematical models used in our implementation. We also give insight to the state of the art of given topics. We note here that x' denotes dx/dt.

1.1 Spatial working memory

Working memory, unlike long-term memory, has limited capacity and is used to maintain memories for a short period of time. For example, this can be relevant for maintaining numbers while they are noted or in a digit-span task [2]. Researchers have associated neural correlates of working memory more and more with the prefrontal cortical areas.

Delayed response paradigms (for comparison, see section 1.1.1), utilized when studying working memory as the ability to remember events for a short period of time in the context of remembering spatial locations, have shown that neurons in the prefrontal cortex are activated for a few seconds after a stimulus vanished. Selective persistent activity of a specific subgroup of neurons depending on the stimulus has, thus, been considered responsible for maintaining the working memory [6, 5, 12]. Moreover, Compte [5] argues that persistent neuronal activity might have been developed as a general strategy used by the nervous system to retain needed information that is no more available to the senses. States of persistent elevated neuronal activity in selected group of neurons might be considered attractor states. In this case, the brain activity in a spatial working memory task may be looked at as an activity of a multistable system able to switch across several stable attractor states depended on the parameters of the sensed environment [5].

Experiments with the *oculomotor delayed-response task* [10] (section 1.1.1) show

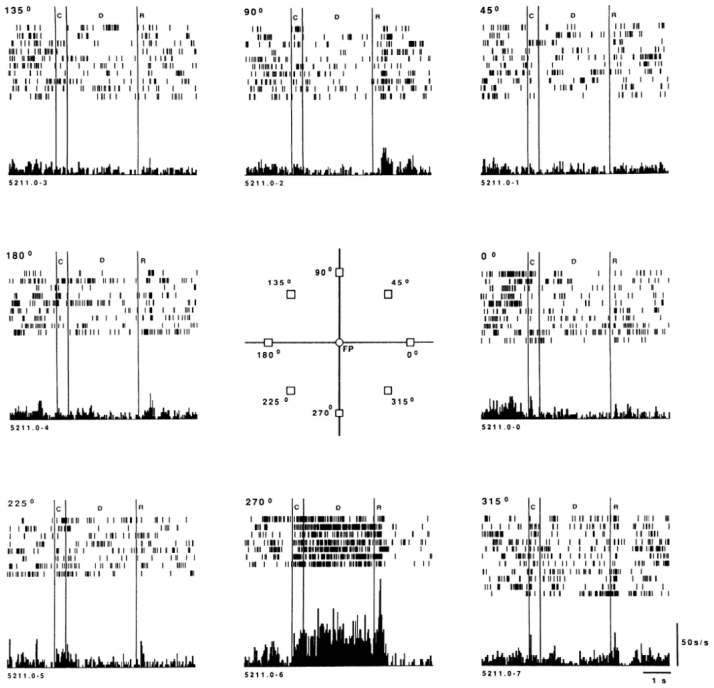

Figure 1.1: Recording of a neuron with preferred cue angle 270°. It is evident that this neuron shows highly elevated activity when presented with a stimulus at 270°. Inhibition of this neuron can be also observed during the presentation of a 90° cue. *Image taken from* [10].

that pyramidal neurons[1] in the dorsolateral prefrontal cortex form *memory fields* related to the location of a presented visual target [12, 19]. The neurons have the maximal firing when the target is presented at one or a few locations in the visual field and one neuron always codes the same location [12]. In relation to the task, the neurons have preferred cue angles. They also show the effect of *opponent memory fields*. Increase in activity of pyramidal neurons with one preferred cue angle causes inhibition of neurons with the opposite preferred cue angle (for comparison, see figure 1.1). This can be illustrated on an example: when the subject is presented with a stimulus at 0°, activity of a particular group of neurons - coding the stimulus location - sharply rises, but activity of neurons coding 180° falls, as was shown experimentally [10].

Goldman-Rakic [12] recognizes neurons that are active during the presentation of a stimulus, those that are active during the subsequent *delay period* (see section 1.1.1) and those that are active during the memory-guided response. However, many neurons are not time-locked to only one of the described periods. She proposes a laminar hierarchy of neurons, assembled according to their function.

In the architecture Goldman-Rakic [12] proposed, pyramidal cells with the same

[1]Pyramidal cells (or pyramidal neurons) are neurons with rich connectivity that contain excitatory neurotransmitter *glutamate*. They are the most populous neuron type in the cortex and comprise approx. 70-90% of all cortical neurons [8].

preferred direction are interconnected and form columns. Interneurons[2] are crucial for this columnar architecture, as they connect pyramidal cells of one column with their antagonistic counterparts within another column. This enables inhibition of the pyramidal cells whose preferred cue direction is opposite to the direction of a stimulus. This feature is in agreement with findings of Funahashi and his colleagues [10]. It has been shown that interneurons also form memory field similar to those formed by pyramidal cells [12, 19].

1.1.1 Oculomotor delayed-response task

Various delayed-response paradigms have been employed to study spatial working memory. In a classical, manual delayed-response task, a monkey was required to find a food reward whose location had previously been shown and then hidden by an opaque screen during the delay period [12].

Funahashi and his colleagues [10] used an *oculomotor delayed-response task*. This task consisted of five periods: inter-trial period (ITI), fixation period (F), cue presentation period (C), delay period (D) and response period (R). After a period of 5 s (ITI), the monkey fixated a central point on a monitor (F). After 0.75 s a visual cue was presented in one of four or eight peripheral locations (P), randomized over trials. This randomization ensured that the monkey could not predict in what location the next peripheral cue would occur. Presentation of the cue lasted for 0.5 s. Fixation had to be maintained until the end of the delay period (D), lasting for 1-6 s. Then, the central fixation point vanished from the screen and the monkey had to do a saccadic eye movement (R). If this movement was done within the next 0.5 s to the location where the cue had been presented (within a window of 6°), the monkey was rewarded. The periods of the oculomotor delayed-response task are visualized in figure 1.2.

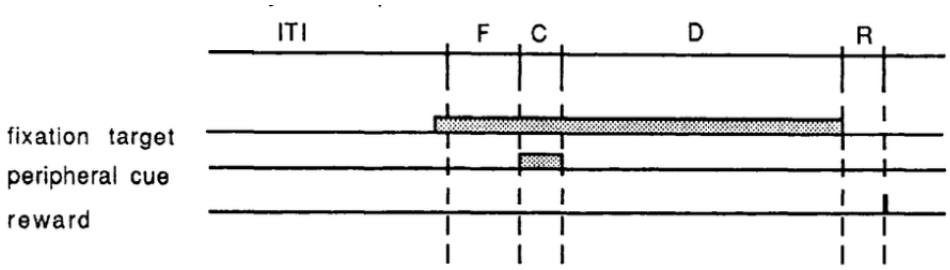

Figure 1.2: Periods of the oculomotor delayed-response task. ITI - inter-trial period, F - fixation period, C - cue-presentation period, D - delay period, R - response period *The illustration taken from* [10]

[2]Interneurons are neurons that contain inhibitory *gamma-aminobutyric acid* (GABA). Their fundamental role is thought to be controlling the level of activity in a particular brain area via inhibition [9].

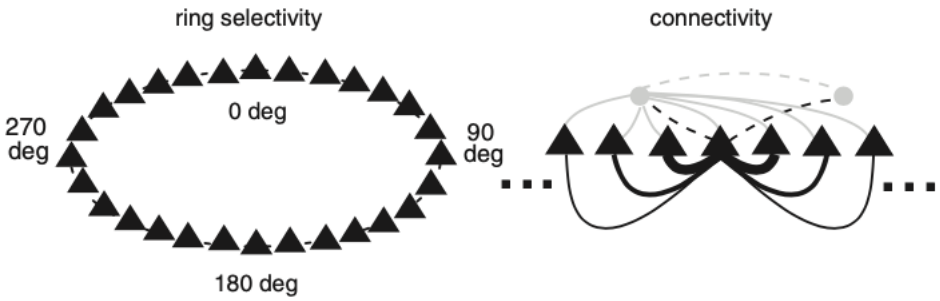

Figure 1.3: A schema of spatial distribution of the neurons on a ring and the connectivity structure between pyramidal cells (black triangles) and interneurons (grey circles). Each black triangle represents a group of pyramidal cells sensitive to the same peripheral angle. *The illustration taken from* [1].

A crucial feature of this paradigm was that the monkey was required to maintain fixation during the delay period. Thus, the monkey's behavior could be controlled with high precision and it was ensured that the monkey had to use working memory to achieve a high level of performance. The scientists could also record the monkey's direction of gaze throughout the task and compare monkey's behavior over trials [10].

1.2 Model of the spatial working memory

Compte and his colleagues [6] used a network architecture which was consistent with columnar organization of dorsolateral prefrontal cortex as described by Goldman-Rakic [12]. The model consisted of excitatory pyramidal cells and inhibitory interneurons. Pyramidal cells were 4 times more numerous than interneurons. Cells were spatially distributed according to their preferred cue angle on a ring (figure 1.3). They modelled the neural cells as *leaky integrate-and-fire units*. External excitatory inputs from other cortical areas were modelled as uncorrelated Poisson spikes to each neuron at rate 1800 Hz per cell (or 1000 Poisson spike trains, each with a frequency of 1.8 Hz). Excitatory inputs to cells were received via $AMPA$ and $NMDA$ receptors and inhibitory inputs via $GABA_A$ receptors.

1.2.1 Leaky integrate-and-fire neuron

Leaky integrate-and-fire neuron is one of the most widely used models in computational neuroscience [15]. Its subthreshold dynamics is described by the following linear differential equation:

$$CV' = I - g_{leak}\,(V - E_{leak}) \tag{1.1}$$

In this equation, C is the total membrane capacitance, V is the membrane potential, g_{leak} is the total leak conductance and E_{leak} is the leak reversal potential. When V

reaches the threshold V_{th}, and action potential is fired. V is then reset to a V_{res} value for the refractory period τ_{res}.

Leaky integrate-and-fire neuron has a well-defined threshold and a relative refractory period. Strength of the input can be continuously encoded in the frequency of spikes, and excitatory inputs ($I > 0$) facilitate firing, whereas inhibitory inputs ($I < 0$) decrease the membrane potential [17].

Izhikevich [17] is critical about this model. Despite being computationally effective, it cannot produce rich spiking and bursting dynamics of cortical neurons and has unwanted mathematical properties. This model does not model a spiking behavior; it is only said that a neuron 'spiked' when the neuron's membrane potential V reaches the threshold value V_{th}.

1.2.2 Details about the model architecture

In the model [6], synaptic responses are modelled according to Wang [26]. In this model, current running to a cell is sum of currents from $NMDAR$, $AMPAR$ and $GABA_AR$ channels. Synaptic current at a receptor:

$$I_{syn} = pg_{syn}s_{syn}\left(v - V_{syn}\right) \tag{1.2}$$

Variable g_{syn} represents the conductance of a receptor. Its value depends on the difference of the preferred cue of connected neurons. It is computed as $g_{syn,ij} = G_{syn}W\left(\theta_i - \theta_j\right)$. G_{syn} is a parameter specific for each type of the receptor. $W\left(\theta_i - \theta_j\right)$ is a constant for unstructured connections and a constant term plus a Gaussian centered at $\left(\theta_i - \theta_j\right) = 0$ for connections structured according to preferred cue angles θ_i and θ_j:

$$W\left(\theta_i - \theta_j\right) = J^- + \left(J^+ - J^-\right)\exp\left(\frac{-\left(\theta_i - \theta_j\right)^2}{2\sigma^2}\right) \tag{1.3}$$

J^- is the strength of the weaker cross-directional connections, whereas J^+ is the strength of the stronger isodirectional connections. σ is the width of the 'connectivity footprint' $W\left(\theta_i - \theta_j\right)$ normalized as:

$$\frac{1}{360}\int_0^{360} W\left(\theta_i - \theta_j\right)d\theta_j = 1 \tag{1.4}$$

Therefore, only J^+ and σ are given as parameters. J^- can be computed according to the *normalization condition* (equation 1.4). Figure 1.4 shows the graph of W.

The variable s_{syn} is the synaptic gating variable, which represents the fraction of opened ion channels. $AMPAR$ and $GABA_AR$ channels have the following opening dynamics with after-spike rises followed by exponential decays with time constant τ:

$$s'\left(t\right) = -\frac{s\left(t\right)}{\tau} + \sum_k \delta\left(t - t_k\right) \tag{1.5}$$

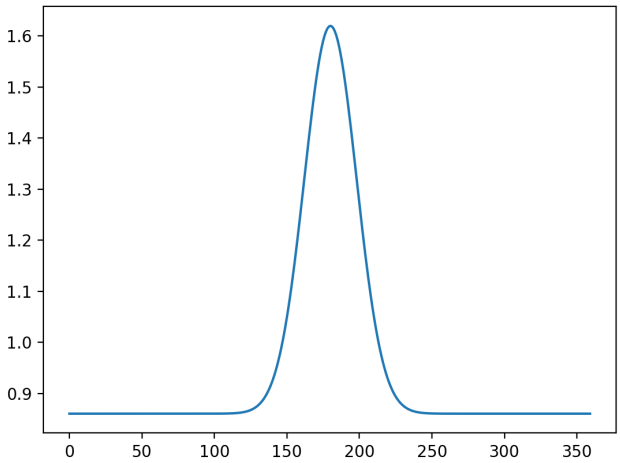

Figure 1.4: Strength of structured connections of pyramidal cells depending on their proximity to the neurons with 180° preferred cue angle according to the *connectivity footprint* (equation 1.3). On the x-axis is shown the preferred cue angle θ and on the y-axis is shown $W(\theta)$. Parameters are chosen as $J^+ = 1.62$ and $\sigma = 18°$.

where t_k denotes time of spike of a presynaptic neuron and δ is the Dirac function. The sum over presynaptic spike times, then, checks whether a spike occured at t. If yes, the synaptic gating variable s_{syn} jumps with magnitude 1 [6]. For $AMPAR$ channels, $\tau_{AMPA} = 2$ ms, and $\tau_{GABA_A} = 10$ ms for $GABA_AR$ channels.

$NMDAR$ channels have different dynamics with slower rises and decays controlled by parameters $\tau_{rise} = 2$ ms and $\tau_{decay} = 100$ ms. Parameter $\alpha = 0.5$ kHz controls the saturation properties of the channel at high presynaptic firing frequencies. The dynamics is described by two differential equations:

$$s'(t) = -\frac{s(t)}{\tau_{decay}} + \alpha x(t)(1 - s(t)) \tag{1.6}$$

$$x'(t) = -\frac{x(t)}{\tau_{rise}} + \sum_k \delta(t - t_k) \tag{1.7}$$

$NMDAR$ channels are voltage dependent, with variable $p = 1/(1 + [Mg^{2+}]\exp(-0.062v/3.57))$, with $[Mg^{2+}] = 1.0$ mM, whereas $p = 1$ for voltage independent $AMPAR$ and $GABA_AR$ channels.

Parameter V_{syn} is the membrane synaptic reversal potential, whose value is the point at which positive current, causing depolarization, becomes negative, causing hyperpolarization.

Number of pyramidal cells (excitatory neurons) in the network [6] is $N_E = 2048$ and number of interneurons (inhibitory neurons) is $N_I = 512$. Recurrent synaptic conductance parameters are denoted G_{EE} for pyramid-to-pyramid, G_{EI} for pyramid-to-

	Compte et al. control parameter set	**Edin et al.**	**Almeida et al.**
G_{EE}	0.381 nS	0.684 nS	0.7 nS
G_{EI}	0.292 nS	0.479 nS	0.49 nS
G_{IE}	1.336 nS	3.643 nS	0.935 nS
G_{II}	1.024 nS	2.896 nS	0.7413 nS
J^+_{EE}	1.62	1.5	
J^+_{EI}	1.25	1.4	
J^+_{IE}	*not used*	1.4	
σ_{EE}	18°	9.4°	
$\sigma+_{EI}$	18°	32.4°	
$\sigma+_{IE}$	*not used*	32.4°	

Table 1.1: Different model parameters used in Compte et al. [6], Edin et al. [7] and Almeida et al. [1]. J^+_{EI} and σ_{EI} used only in some simulations of Compte and his colleagues [6]. Note that Edin et al. [7] and Almeida et al. [1] share the same parameters used in the connection footprint.

interneuron, G_{IE} for interneuron-to-interneuron and G_{II} for interneuron-to-interneuron connections. If different number of neurons is used, synaptic conductances are scaled inversely propotional to $N_E + N_I$. This allows for keeping the total level of synaptic conductance unchanged. In most simulations, $AMPAR$-mediated channels are not involved and only the pyramid-to-pyramid connectivity is structured according to the preferred cue angle. Interneuron-to-interneuron are not structured in any simulations. Inhibition is stronger than excitation and $G_{IE}/G_{EE} = G_{II}/G_{EI}$.

Compte and his colleagues [6] used two different parameter sets. Parameters used in the *control parameter set* are listed in table 1.1.The *modulated parameter set* is similar to the control parameter set, except for enhancement in conductances ($G_{E\{E,I\},m} = 1.2G_{E\{E,I\}}$, $G_{I\{E,I\},m} = 1.4G_{I\{E,I\}}$).

Parameters for the *connectivity footprint* are also included in table 1.1. Pyramid-to-interneuron connections were structured only in some simulations.

A similar model was used by Edin et al. [7] and Almeida et al. [1]. Here, all but interneuron-to-inerneuron connections were structured. Connectivity between excitatory and inhibitory neurons was wider and flatter than between excitatory neurons. Parameters used in both studies are shown in table 1.1.

1.2.3 Simulation of the oculomotor delayed-response task

The simulation protocol [1, 6, 7] followed the *oculomotor delayed-response* protocol employed by Funahashi and co-authors [10].

During the presentation period, selective transient current was injected to pyramidal cells with preferred cues close to the stimulus angle. Stimulation input to a cell with preferred cue angle θ can be computed as [1, 7]:

$$I_{stim}\left(\theta, \theta_{stim}\right) = \alpha \exp\left(\mu\left[\cos\left(\frac{2\pi}{360}\left(\theta - \theta_{stim}\right)\right) - 1\right]\right) \tag{1.8}$$

θ_{stim} is the presented cue angle, and the strength of the selective transient current $I_{stim}\left(\theta, \theta_{stim}\right)$ decreases as $(\theta - \theta_{stim})$ increases. Parameter $\alpha = 0.025$ nA represents the highest delivered input current strength (peak value) and $\mu = 39$.

No selective transient currents are presented during the delay period. Oculomotor response in the response period is simulated as a current injection to all neurons in the network.

During the presentation period, the network [6] builds elevated activity of neurons with the preferred cue close to the stimulus. This activity persists during the delay period because of reverberatory loops. Cells around the location of the stimulus show strong excitatory feedback. Profile of this elevated activity does not depend on the exact shape or intensity of the stimulus and the network goes into a 'bump' state.

Non-selective stimulus to all neurons during the response period causes the network to *switch off*. It is due to strong inhibitory feedback, which builds up to be strong enough to calm down all the excitatory activity of the pyramidal cells.

Development of the network activity is shown in figure 1.5.

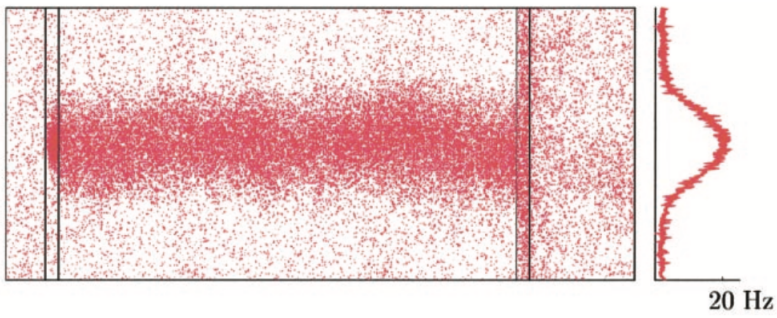

Figure 1.5: Rastergram of neural spiking shows elevated spiking activity during the delay period in neurons with preferred cue close to the stimulus ('bump' state). This activity starts when the selective transient current is being injected to these neurons, persists during the delay period when the selective transient current is missing and vanishes when the transient current is injected to all neurons. The time step in the simulation was 0.02 ms. *Image taken from* [6].

1.2.4 Distractors

Some trials of the experiment [6] were done with distractors presented during the delay period. These were of the same intensity and length as the original stimulus, but in

different peripheral locations. The impact of distractors on the network was measured by the drift of the peak location of the enhanced neuronal activity after the distraction.

It was observed in the simulations that the resistance of the network to the distractors depended on the strength of the stimulus. Sufficiently large amplitude of the stimulation current could overcome the 'bump' state dynamics of the neuronal activity in the network and move its peak closer to the distractor location. The network with enhanced conductances (the modulated parameter set - see section 1.2.2) was more resistant to distractors [6]. These dependencies can be seen in figure 1.6.

Last but not least, the amount of distraction also depended on the proximity of the location of the original stimulus and the distracting stimulus. For distractors close to the original cue angle, the distraction rose almost linearly with the distance. It reached its maximum at approx. 90° distance of the angles. When the two angles were farther apart than 90°, the distraction became small [6].

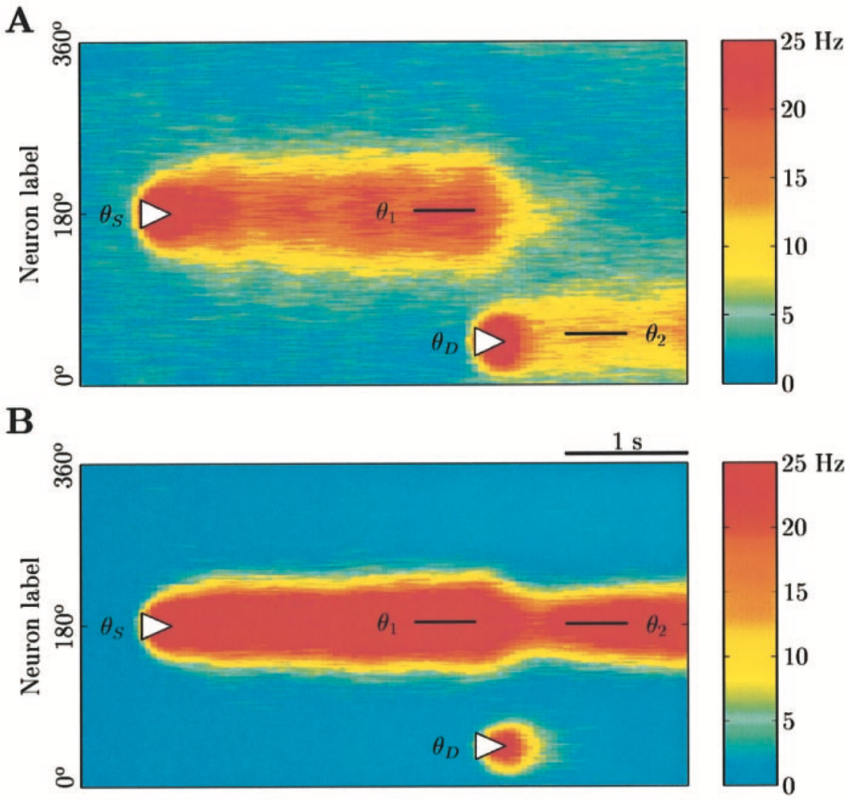

Figure 1.6: Stimulus intensity affects the network's resistance towards distractors. In *A*, the control parameter set network is completely distracted when a stimulus of 200 pA is used. When a stimulus of 100 pA is used, the modulated parameter set network remains undistracted in *B*. *Image taken from* [6].

1.2.5 Spatial working memory model related research

While Compte and his colleagues [6] described the model of spatial working memory and tested it on a series of experiments comparing it to neuronal records of Funahashi and colleagues [10], the model has been put into practice and used in several other scientific studies.

Edin and his colleagues [7] used the model of spatial working memory to simulate the intraparietal sulcus, an area thought to be responsible for storage of short-term memories, in a study on the function of the dorsolateral prefrontal cortex in top-down control of the working memory capacity. They used the model in which all internal but inhibitory-to-inhibitory connections were spatially tuned (for comparison, see section 1.2.2). In the presented model, the spatially tuned network representing the intraparietal sulcus received unspecific excitatory inputs from the network representing dorsolateral prefrontal cortex, whose connectivity was not spatially tuned. The authors of the study presented a mathematical model explaining the mechanisms behind the capacity of the visuospatial working memory, supported by the empirical data.

Another study using the model of spatial working memory is by Almeida and her co-authors [1]. In this study, the authors used the model to investigate the memory of multiple items. The study focused on how proximity of spatial locations of several memorized items influence the precision of their recall. The study confirmed that the items were recalled with attractive or repulsive recall bias, based on how close they were to each other.

The spatial working memory model has also been subject to a theoretical paper by Compte [5]. In the paper, the author discussed the model of the spatial working memory within the attractor theory framework. The author also discussed the biological relevance of the mechanisms of the working memory model and pointed out the biologically observed increased variability of neurons' spike trains during the persistent elevated activity, a feature very difficult to be accounted for in the computational models. The models, on the other hand, showed a more regular activity.

Exercises accompanying the book *Neuronal dynamics: From single neurons to networks and models of cognition* [11] contain an implementation of the model of spatial working memory [6] used for educational purposes. The exercise[3] uses different parameters than in the publication by Compte and his colleagues [6], but it enables its user to observe different properties of the model.

[3]This exercise is directly available at the webpage: `neuronaldynamics-exercises.readthedocs.io/en/latest/exercises/spatial-working-memory.html`.

1.3 Simple model of spiking neurons

Izhikevich [14] proposed a computationally efficient model that can produce large variety of firing patterns of cortical neurons. Based on bifurcation theory [17], this model consists of four parameters and a two-dimensional system of ordinary differential equations:

$$v' = 0.04v^2 + 5v + 140 - u + I \tag{1.9}$$

$$u' = a\,(bv - u) \tag{1.10}$$

where the values of v and u are reset when a spike occurs:

$$\text{if } v \geq 30 \text{ mV, then } \begin{cases} v & \longleftarrow c \\ u & \longleftarrow u + d \end{cases} \tag{1.11}$$

In the equations, the parameters a, b, c and d work as dimensionless variables. Variable v represents the membrane potential and u represents a membrane recovery variable, relating to the activation of K^+ and inactivation of Na^+ ionic currents. Parameter a is the time scale of the recovery of u. Parameter b represents sensitivity of u to subthreshold fluctuations of v. Parameter c is the after-spike reset value of v and d is the after-spike reset value of u. It is to be mentioned that 30 mV is not the threshold value of the spike, it is the peak of the spike. The threshold is dynamical, like it is in biological neurons, and it lies between -70 mV and -50 mV.

These parameters can be chosen in different ways to simulate behaviors of different types of neurons. Typical values of each parameter are $a = 0.02$, $b = 0.2$, $c = -65$ mV and $d = 2$.

Excitatory and inhibitory neurons in the mammalian brain are divided into several classes. These can be simulated by the *Simple model of spiking neurons* and are described by Izhikevich [14]. Here, we describe *regular spiking* and *fast spiking* neurons, since they are used in this thesis.

1.3.1 Regular spiking neurons

Excitatory regular spiking (RS) neurons are the most common type of neurons found in the mammalian brain. They are found as stellate and pyramidal cells [17]. When they are stimulated with a prolonged stimulus, they fire a few spikes with higher frequency and this frequency then decreases. This process is called *spike frequency adaptation*. Simulation of spiking of a RS neuron can be seen in figure 1.7. The spiking frequency slightly increases with stronger stimulation. This type can be achieved with $a = 0.02$, $b = 0.2$, $c = -65$ mV and $d = 8$ [14]. The initial values $v_0 = -90$ mV and $u_0 = bv_0$.

We have observed that the neuron fires when instantaneous depolarization reaches $v_t > -56$ mV.

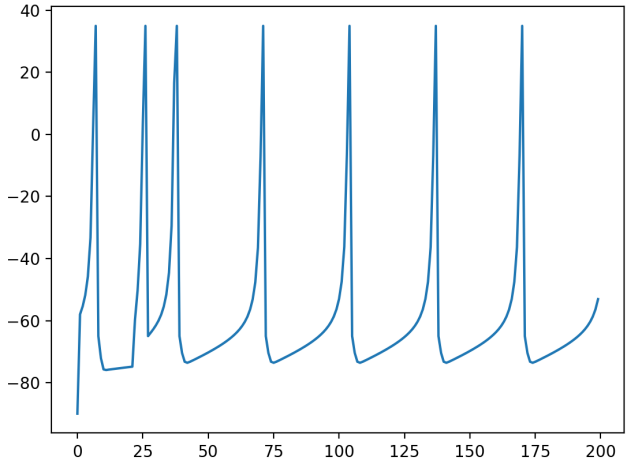

Figure 1.7: Simulation of a regular spiking neuron with the Simple model of spiking neurons [14]. The graph shows the time development of the membrane potential $v(t)$ for a period of 200 ms. The time step is 1 ms.

1.3.2 Fast spiking neurons

Fast spiking (FS) neurons are inhibitory neurons, morphologically including basket or chandelier cells (types of interneurons). They provide local inhibition along the *intralaminar* (horizontal) direction of the neocortex [17]. They fire periodically with a very high frequency and exhibit no frequency adaptation (figure 1.8). This can be obtained with fast recovery, corresponding to $a = 0.1$. The other parameters are: $b = 0.2$, $c = -65$ mV and $d = 2$ [14]. The initial values $v_0 = -90$ mV and $u_0 = bv_0$.

1.3.3 Simple model of spiking neurons related research

Izhikevich described the Simple model of spiking neurons extensively in several of his research papers. He defined the model and discussed its potential use [14], compared it to other models of neurons [15] and explaind thoroughly on which concepts the model was based [17]. Izhikevich [16] studied the self-organization of spiking neurons into neuronal groups. He implemented a large neuronal network inspired by the cerebral cortex. The study showed how the Simple model of spiking neurons can be used to build large brain networks.

The model has found its place in the field of computational neuroscience. In a research of Wacongne and her colleagues [25], the Simple model of spiking neurons was used to computationally model auditory cortex based on predictive coding. Similarly to

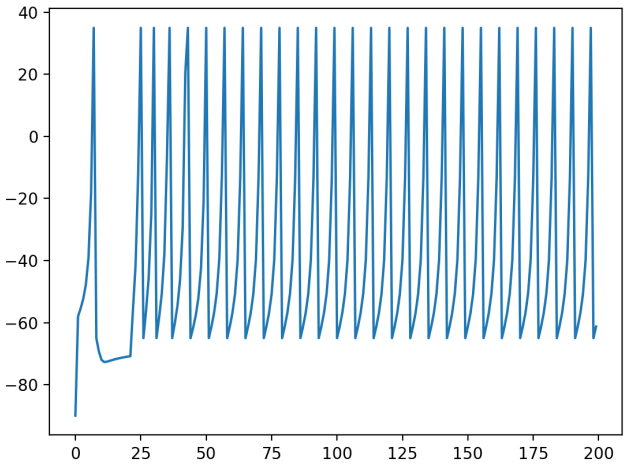

Figure 1.8: Simulation of a fast spiking neuron with the Simple model of spiking neurons [14]. The graph shows the time development of the membrane potential $v(t)$ for a period of 200 ms. The time step is 1 ms.

the model of spatial working memory [6], synapses were modelled according to Brunel and Wang [3]. Therefore, the implementation of Wacongne and the co-authors [25] represents an example of a larger network architecture in some aspects similar to the model of spatial working memory [6] built using the Simple model of spiking neurons [14].

One of the most related studies to out thesis is by Szartmáry and Izhikevich [20]. In this study, the simple spiking neurons [14] were used to simulate working memory in an attempt to relate the precise spike timing of events in the brain to emergence of working memory functionality. In this model, memories were represented as overlapping neuronal groups with stereotypical, yet not necesarilly synchronous time-locked firing patterns. These patterns, called *polychronous* patterns, were defined by synaptic patterns, which meant that a neuron could be included in different polychronous patterns. Unlike the work of Compte and his colleagues [6], neuronal groups were not defined by the strength of synaptic connections, but by the exact timings of axonal conduction delays arranged in a way that enabled for different functional subnetworks.

Chapter 2

Motivation and goals

The model of the spatial working memory [1, 6, 7] was originally implemented using the computationally effective leaky integrate-and-fire units (see section 1.2.1) as a neuron model. According to Izhikevich [14, 15, 17], this model of a neuron was very limited in the number of types of neurons it could simulate and had mathematical 'flaws' in terms of simulating the spiking dynamics. Therefore, it might be beneficial to implement the model of spatial working memory employing a more general model of a neuron; a model which can simulate a broad range of types of neurons. The Simple model of spiking neurons by Izhikevich [14] is suitable for the task because not only can it simulate multiple types of neurons, it is also computationally effective (see 1.3).

The main goal of this thesis is to see how the model of spatial working memory can be implemented employing the Simple model of spiking neurons, and to see how it needs to be tuned in order to be able to simulate the oculomotor delayed-response task (see section 1.1.1) experiments and obtain similar results to those of simulations of Compte and his colleagues [6].

More specifically, we are looking for these features of the network, observed in the original implementation of the model of spatial working memory [6]:

1. The ability of the network to develop a selective spiking activity of the neurons whose preferred cue angle is close to the angle of the stimulus. This activity persists even after the stimulus vanished.

2. The ability of the network to switch off to the basal state when the whole network is stimulated by a strong stimulus.

These two features of the spatial working memory model are visible on the rastergram figure 1.5.

Additionally, we are looking at how our implementation deals with distractors. The original implementation showed varied behavior depending on the proximity of the original stimulus presented during the cue presentation period and a distractor

presented during the delay period, and on the strength of the stimulus (the same strength was used for both the original stimulus and the distractor) [6]. It was also observed that an increased strength of connections in the network enabled it to be less prone to distraction. Section 1.2.4 discusses distractors in more detail.

Chapter 3

Implementation of the model

The main practical task of our Master's thesis is implementing the model of the spatial working memory [1, 6, 7] using the Simple model of spiking neurons [14]. We decided to do the implementation in *Python 2* [23]. We used packages `numpy`, `mathplotlib.pyplot`, `math` and `csv`.

Our task consisted of implementing the Simple model of spiking neurons [14], the connectivity between the neurons in the network and the simulation protocol.

3.1 Neuron

The neuron properties are defined as a dictionary where `"a"`, `"b"`, `"c"` and `"d"` correspond to the neuron parameters defined by the Simple model of spiking neurons [14] and `"v_0"` represents the initial value of the membrane potential v_0 (u_0 has to be computed as $u_0 = bv_0$; for comparison see section 1.3). Initiation of each type of the neuron is done by the function `init`, which takes 5 arguments `a`, `b`, `c`, `d` and `v_0`.

Equations 1.9, 1.10 and 1.11 are implemented in the `update` function using the forward Euler method [28]. According to this method, $x(t+\tau) = x(t) + \tau f\left(x(t)\right)$ for a differential equation $x' = f(x)$. Using this method:

$$v(t+\tau) = v(t) + \tau\left(0.04v(t)^2 + 5v(t) + 140 - u(t) + I\right) \tag{3.1}$$

$$u(t+\tau) = u(t) + \tau\left(a\left(bv(t) - u(t)\right)\right) \tag{3.2}$$

.

In these equations, t represents the current time in ms and τ represents the time step in ms.

The `update` function outputs are 3-tuple. The first value is the neuron's updated membrane potential v, the second one is the updated membrane recovery variable u and the third one is a binary value signaling whether or not the neuron fired.

The neurons in the network are represented by three matrices of size $N \times T$ where $N = N_e + N_i$ represents the number of excitatory and inhibitory neurons in the network

and T represents the number of steps of the simulation (total experiment time divided by the time step). Matrix `v` (matrix `u`) stores the values of the membrane potential $v(t)$ (membrane recovery variable $u(t)$) in every simulation step, so that `v[i][t]` (`u[i][t]`) stores the value of the membrane potential $v_i(t\tau)$ (the membrane recovery variable $u_i(t\tau)$) of the neuron i ($0 \leq i < N$) at the simulation time $t\tau$ ($t \in \mathbb{N}$ and $0 \leq t \leq T/\tau$). The array `inp`, constructed in a similar manner, represents the input current I to the neuron i. Other neuron related arrays related in the network are `just_fired` and `num_of_firings`. These two arrays are, more specifically, related to the firings of the neuron. In the former one, `just_fired[i]` is set to 1 when the neuron i fired in the current simulation step, otherwise it is set to 0, and the latter one counts the number of firings for every neuron in the network.

Index i related to the neurons in the network represents an excitatory neuron when $0 \leq i < N_e$, and an inhibitory neuron when $N_e \leq i < N$.

3.2 Network architecture and connectivity

Pyramidal neurons in the model are spatially distributed on a ring, covering the circle [6]. In our implementation, we divide pyramidal neurons into groups with preferred cue angles according to their indices $i \in \mathbb{N}$. If $q \in \mathbb{N}$ is the number of preferred cue angles, then $\theta_i = (i \bmod q)\,\frac{360}{q}$ is the preferred cue angle of the neuron i. This division is not completely equal for every angle in the network, but it can be seen that there is no more than one extra neuron for some angles. We call this assignment of neuronal labels *non-uniform*. We also use an equal spread of the neurons, characterized by the equation $\theta_i = \frac{360}{N_e} i$, in some of the simulations. N_e is the number of excitatory pyramidal cells. We call this assignment of neuronal labels *uniform*.

Each neuron in the network receives a sum of synaptic currents I_{syn} originating in other, presynaptic, neurons (equation 1.2). Each synaptic current depends on the strength of the connection between the presynaptic and the postsynaptic neuron.

Connections between all the neurons in the network are represented in the *connection matrix* `g`. For each two neurons i and j, `g[i][j]` represents the strength of the connection from the (presynaptic) neuron i to the (postsynaptic) neuron j. Each `g[i][j]` is, then, equivalent to the receptor conductance variable $g_{syn,i,j}$ (section 1.2.2).

According to the model [6, 1], connections between some neurons are spatially tuned (see section 1.2). It means that the strength of a connection between two neurons i and j depends on the proximity of their preferred cue angles. This is reflected by the *connectivity footprint* (equation 1.3). The connectivity footprint of two neurons is implemented in the function `W_conn_foot`. In this function, J^+ and σ are parameters defined by the network properties, and J^- needs to be computed according to the

normalization condition (equation 1.4). The normalization condition is in the form of a definite integral, which we compute as:

$$\int_0^{360} W\left(\theta_i - \theta_j\right) d\theta_j =$$
$$\int_0^{360} \left[J^- + \left(J^+ - J^-\right) \exp\left(\frac{-\left(\theta_i - \theta_j\right)^2}{2\sigma^2} \right) \right] d\theta_j =$$
$$\left[\theta_j J^-\right]_0^{360} + \left(J^+ - J^-\right) \int_0^{360} \exp\left(\frac{-\left(\theta_i - \theta_j\right)^2}{2\sigma^2} \right) d\theta_j =$$
$$360 J^- + \left(J^+ - J^-\right) \underbrace{\int_0^{360} \exp\left(\frac{-\left(\theta_i - \theta_j\right)^2}{2\sigma^2} \right) d\theta_j}_{\mathscr{I}(\theta_i)}$$

The next step is to compute the integral marked as $\mathscr{I}(\theta_i)$. It can be done using the Error function [27] already implemented in `math` package as `math.erf`:

$$\mathscr{I}(\theta_i) = \int_0^{360} \exp\left(\frac{-\left(\theta_i - \theta_j\right)^2}{2\sigma^2} \right) d\theta_j =$$
$$\frac{1}{2}\sqrt{\pi}\sigma^2 \left(\operatorname{erf}\left(\frac{\theta_i}{\sigma^2} \right) - \operatorname{erf}\left(\frac{\theta_i - 360}{\sigma^2} \right) \right)$$

In the next step, we are able to compute J^- for each angle θ_i from the *normalization condition* as:

$$J^-(\theta_i) = \frac{360 - \mathscr{I}(\theta_i) J^+}{360 - \mathscr{I}(\theta_i)} \tag{3.3}$$

Computations of $\mathscr{I}$ and J^- are implemented in functions `W_integral` and `J_minus`.

Synaptic currents I_{syn} also depend on the synaptic channels (section 1.2.2). An important biological feature of synaptic channels is their dynamics dependent on the spiking activity of the presynaptic neuron. The dynamics of $AMPAR$ and $GABA_AR$ channels are described by the equation 1.5. For the sake of immediate clarity, these $AMPAR$ and $GABA_AR$ channel dynamics are implemented in two separate functions `ds_AMPAR` and `ds_GABAR`[1]. The more complex dynamics of $NMDAR$ channels described by equations 1.6 and 1.7 are implemented in functions `ds_NMDAR` and `dx_NMDAR`. These three equations are in the form of differential equations, so we used the forward Euler method [28] to compute the derivative. These equations include sums over the presynaptic spike times [6, 25]. We implement these sums through the binary variable `just_fired[i]`, set to 1 when the presynaptic neuron i fired an action in the previous simulation step, and 0 otherwise. This mimics the after-spike rising dynamics

[1]This might not represent the most efficient solution from the programmer's viewpoint. As we see, the two functions implement the same equation, which differs only by the constant τ.

of the channels [6, 25]. Synaptic current I_{syn} delivered via the $NMDAR$ synapses is multiplied by the factor p implemented in function `NMDAR_factor` (see section 1.2.2).

In some of the simulations, we use the sign control for the synaptic input current value I_{syn}, depending on whether the input came a excitatory or inhibitory synapse. We introduce a condition that if the synapse is excitatory (inhibitory), the resulting I_{syn} cannot be less (greater) than zero. That means that if it were, I_{syn} would be set to zero.

We use two forms of the synaptic current equation. Alongside the form shown in equation 1.2, we use the synaptic current equation:

$$I^*_{syn} = pg_{syn}s_{syn}\left(V_{syn} - v\right) \tag{3.4}$$

We call this equation the *inverse definition* of the synaptic current and label it I^*_{syn}. Such a definition of the synaptic current was chosen following the manner in which equation was presented by Izhikevich [17].

We do not use $AMPAR$ channels in modelling internal synaptic activity, following work of Compte and his colleagues [6]. Channel dynamics of all used internal synaptic channels is stored in array `s`, where `s[i]` represents the current value of the synaptic gating variable s for each presynaptic neuron i. Similar array `x` is used for the variable x (see equation 1.7).

Random number generator `random.random` is used to generate uncorrelated Poisson spikes at a given average frequency f. A Poisson spike is delivered in a given simulation step t when a random constant $rand < \frac{f}{1000/\tau}$. The underlying idea is that $1000/\tau$ is the number of 'slots' in ms contained in 1 s. This is implemented in the function `Poisson`.

3.3 Simulation protocol

The simulation protocol is implemented as a `for` cycle through all stimulation steps t such that $0 \leq t < T/\tau$. The cycle can be divided into two functional parts.

In the first part, all the neurons receive their input. It consists of Poisson spike trains, external stimulation current and synaptic input currents. Time parameters t_0, t_p, p_d, t_s and t_e mark lengths of oculomotor delayed-response paradigm phases (section 1.1.1) in their respective order in ms, where t_0 is the pre-trial period and t_e is the post-trial period.

We use much lower frequency than used by Compte et al. [6]. Our frequency f is not higher than 1.8 Hz. This is mostly related to the fact that a much wider time step size is used.

During the cue presentation period, lasting when $t_0/\tau \leq t < (t_0 + t_p)/\tau$, selective transient current $I_{stim}(\theta, \theta_{stim})$ is delivered to the excitatory neurons following equation 1.8. In this equation, α is the peak stimulation current, delivered to the neuron whose

preferred cue angle $\theta = \theta_{stim}$, where θ_{stim} is the presented cue angle. Transient current is implemented in function `I_transient_current`. The value of the parameter α is stored in the variable `i_transient`.

During the response period characterized by $(t_0 + t_p + t_d)/\tau \leq t < (t_0 + t_p + t_d + t_s)/\tau$, all the neurons in the network are stimulated by the transient current of the same strength. The value of this response period current is stored in the variable `i_response`.

During the whole stimulation, all the neurons in the network collect synaptic currents coming from all the other neurons, following connectivity described in section 3.2.

In the second part, all the neurons update their v and u using the `update` function. The `update` function's output is stored in the `v` and `u` matrices. Also $NMDAR$ and $GABA_AR$ channel gating variables s and x are updated. One part of the `update` function output, signaling whether the neuron had just fired, is used to update the channel gating variables.

The time complexity of the simulation protocol is $O(TN^2)$, where T is the number of simulation steps and N is the overall number of neurons in the network. For $T = 5000$ and $N = 640$, a simulation runs for about 1.5 hours on a `2,7 GHz Dual-Core Intel Core i5` *MacBook Pro* portable computer.

3.4 Data collection and analysis

During each simulation, we recorded the membrane potential development, the membrane recovery variable and a number of spikes in each simulation period of a neuron in each cue angle group and of all interneurons as `.csv` files. At the end of each simulation period, we calculated the spiking rate of these neurons. We also kept log files to see how the experiments proceeded. In one of the log files, each stimulation step had its row `[time] : [input_current_stimulated] / [v_stimulated] / [u_stimulated] - [input_current_not_stimulated] / [v_not_stimulated] / [u_not_stimulated] - [input_current_interneuron] / [v_interneuron] / [u_interneuron]` in which we stored inputs, membrane potentials and membrane recovery variables of a stimulated neuron, a neuron with the opposite preferred cue angle, and a randomly selected interneuron to see the activity of interneurons. We also had two log files (one for pyramidal cells and one for interneurons) in which we recorded simulation times in the form $t\tau$ at which the respective neurons fired. This information was stored as a 2-tuple $(t\tau, i)$, where i is the neuron index. Two other log files were used to record the firing frequencies of all pyramidal cells and all interneurons in the delay period.

After the simulation, plots of the membrane potential of the simulated neuron, the

opposite neuron and the interneuron were generated using the `matplotlib.pyplot` Python package. Rastergrams of spike times of the neurons and some other charts were created in the programming language *R* [18] or using the online tool *Plotly Chart Studio* [13].

Chapter 4

Simulations

Our second task was to manipulate parameters of the model to try different solutions and find out how the model can be tuned to simulate the oculomotor delayed-response task (see section 1.1.1).

We identified the connectivity parameters (G_{EE}, G_{EI}, G_{IE} and G_{II}), the connectivity footprint parameters of spatially tuned connections (J_{EE}, J_{EI}, J_{IE}, J_{II}, σ_{EE}, σ_{EI}, σ_{IE} and σ_{II}) and the peak stimulation current amplitude α (equation 1.8) as the parameters to be manipulated.

We tried two different network configurations: the network where only excitatory-to-excitatory connections were spatially tuned [6], and the network with all but inhibitory-to-inhibitory connections spatially tuned [7, 1].

We looked at whether the network was able to develop a persistent selective elevated neural activity of stimulated neurons and whether the network was able to switch off (see section 2). We also tried to figure out how the network deals with the distractors presented during the delay period (see sections 1.1.1 and 1.2). Here we present experiments that were at least partially successful, i.e. in which we managed to succeed in at least one of our research goals. We describe the simulations according to their similar behavioral characteristics.

In the following sections, parameters are presented dimensionless, following the way in which they were treated in the code.

4.1 Simulations with 1 ms time step

In the presented simulations, we used a network with a 4 times smaller number of neurons than used by Compte et al. [6] ($N_e = 512$ and $N_i = 128$). This was possible when all the strengths of the connections were adjusted by a constant factor inversely proportional to the total number of neurons [6]. In this case, the factor was 4. The time step used in the experiment was 1 ms. The parameter set used was the control

parameter set used in the original publication [6], with the absolute values of the channel conductances G multiplied by 4×10^{-3}. We used the inverse definition of the synaptic current (equation 3.4). Our reason for this was that the synaptic reversal potential of inhibitory neurons $V_{syn} = -70$ in Compte et al. [6]. Intuitively, inhibitory synaptic current should lower the whole synaptic stimulation when the membrane potential v of inhibitory neurons is high. In these simulations, we used the non-uniform label distribution with the number of preferred cue groups $q = 90$.

We managed the network to build up persistent elevated activity of strongly stimulated neurons. When a strong transient current stimulation was introduced to the neurons, these neurons built up a high frequency spiking activity which persisted even after the stimulus vanished. We managed to build such activity with the peak stimulation current $\alpha \geq 68.3$. This persistent activity can be characterized by a regular firing pattern of the neurons whose preferred cue angle equaled the presented cue angle. This was presumably caused by the persisting neuron membrane recovery variable u built-up during the cue presentation period. Such a behavior can be seen in figure 4.1. If u was not high enough at the end of the cue presentation period, u gradually fell down, causing the neuron not to spike.

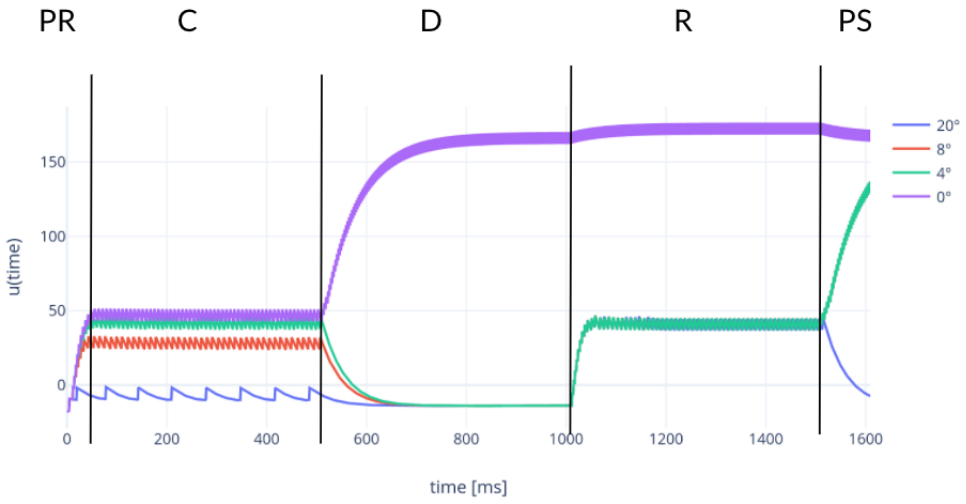

Figure 4.1: Time development of the membrane recovery variable u of neurons at 0°, 4°, 8° and 20°. Stimulation cue angle $\theta_{stim} = 0°$. PR is the pre-trial period (10 ms), C the cue presentation period (500 ms), D the delay period (500 ms), R the response period (500 ms) and PS marks the post-trial period (100 ms).

The overall behavior, seen in the rastergram figure 4.2, shows an elevated activity in a subpopulation of the pyramidal cells during the cue presentation period. This activity even reduced to a smaller subpopulation of neurons during the delay period. A strong elevation of activity, which persisted even after the cessation of the stimulus,

did not disappear in the response period.

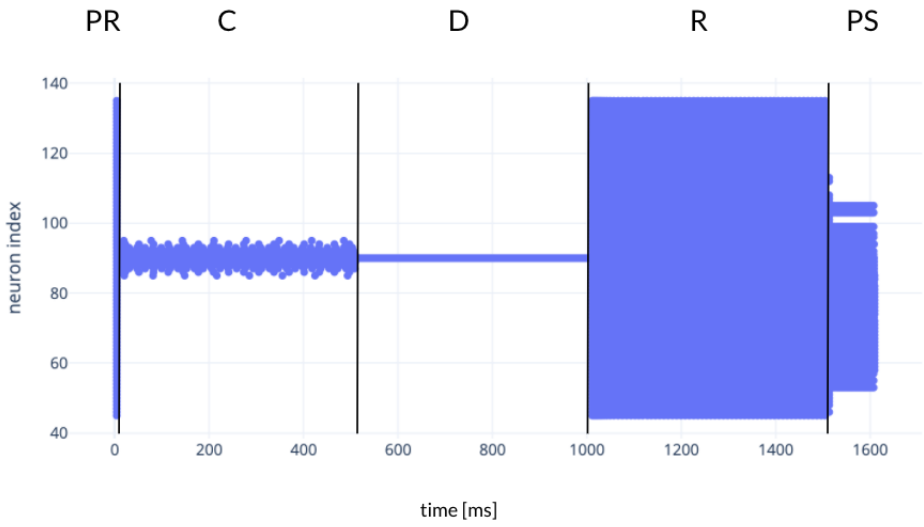

Figure 4.2: Rastergram of the neural activity in the network. Stimulation cue angle $\theta_{stim} = 0°$. We used non-uniform distribution with 90 preferred cue angles (separated by 4°). This graph shows just a subpopulation of networks. The whole network activity consists of patterns repeating along the y-axis (not shown in the figure) due to the nature of the neuronal label distribution. PR is the pre-trial period (10 ms), C the cue presentation period (500 ms), D the delay period (500 ms), R the response period (500 ms) and PS marks the post-trial period (100 ms).

We concluded that the issue with this type of the network was that the persistent activity could not be switched off in the response period even if significantly stronger stimulation current was applied in the response period. On the other hand, activity of a neuron which was not originally stimulated, and which was supposed to be inhibited by the protocol, built up during the response period, in which the neuron was also stimulated. The response period stimulation current amplitude equaled α. However, we can see that the spiking activity of this opposite cue angle neuron did not persist after the response period (figure 4.3).

We assumed that the overall network connectivity was weak and, therefore, the neurons could not influence each other sufficiently. This was accounted for by the lack of spiking activity of the interneurons. All the spiking activity was concentrated in a small subpopulation of pyramidal neurons with preferred cue angle close to the presented cue.

In the next experiments, we, therefore, tried to increase the overall connectivity in the network to see how it affected the network's behavior.

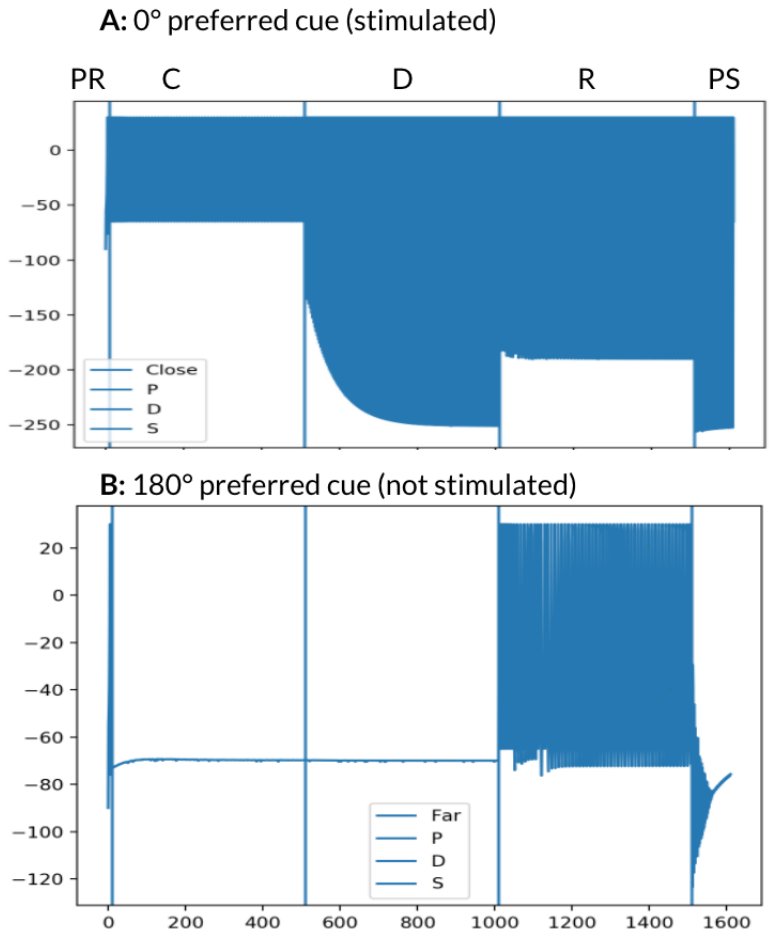

Figure 4.3: Time development of the membrane potential v of a stimulated neuron with preferred cue angle 0° (**A**) and a neuron that was not stimulated with preferred cue angle 180° (**B**). Stimulation cue angle $\theta_{stim} = 0°$. PR is the pre-trial period (10 ms), C the cue presentation period (500 ms), D the delay period (500 ms), R the response period (500 ms) and PS marks the post-trial period (100 ms).

4.2 Strengthening the channel conductance parameters

To increase the activity of the network, we decided to increase the strengths of the connections compared to simulations described in section 4.1, while all other parameters remained the same. We did so by multiplying the channel conductance variables G by factor 4×10^{-2}. When the connections became ten times stronger compared to simulations described in section 4.1, the network displayed spiking activity in almost all time steps. This did not result in the desired outcome and we concluded that the time step 1 ms should be lowered.

4.3 Searching for the optimal parameter set

We observed several facts. One of them was that in Compte et al. [6], the current injected during the response period was of a greater strength than the strength of the selective transient current injected during the cue presentation period. Also, the time step we used previously, 1 ms, could supposedly not simulate the network with enough precision. We, therefore, gradually lowered the time step to 0.2 ms. This allowed us to increase the channel conductances G, as the values leading to persistent elevated activity in simulations described in section 4.1 did not result in the 'bump' state when a lower time step than 1 ms was used.

Here, we present simulations run with 0.2 ms time step and a network four times smaller than the network described by Compte and his colleagues [6]. In a standard simulation, cue presentation started after 100 ms, lasted for 250 ms followed by a delay period of 350 ms. Length of the subsequent response period was 250 ms. With time step 0.2 ms used, this meant that the pre-trial period was from simulation step 0 to 500, the cue presentation period lasted until simulation step 1750, the delay period until 3500 and the response period until 4750. Different simulation lengths are, otherwise, noted. The length of stimulation periods (250 ms) was chosen in accord with Compte et al. [6].

As in simulations described in previous sections, the channel conductances used were in the form $4 \times G_{\{E,I\}^2} \times 10^e$, where $e \in \mathbb{R}$ and $G_{\{E,I\}^2}$ represent the control parameter set conductances (see section 1.2.2). We were gradually increasing the exponent e and observing how it affected the behavior of the network. We present simulations performed with some of the exponents. We observed how different values of J^+ influenced the network's activity. We also manipulated the external and Poisson input current values. The peak value of the selective transient current injected during the cue presentation period α ranged between 2 to 100. We also tried different values of μ (see equation 1.8). The current injected during the response period to all the neurons was chosen to be 4α. We used the Poisson input of values 2 or 20. Both uniform and non-uniform neuron label distributions were tested. Where uniform distribution was used, the number of cues was set to 360. Regarding the synaptic current, sign control was used in some simulations, and some simulations were done with the synaptic current equation 1.2 and some with the inverse form equation 3.4 (see section 3.2).

We present the most significant simulations in the following sections.

4.3.1 Influence of the synaptic current

In order to find out how the synaptic current properties directly influence the network's activity, we simulated the network with synaptic currents computed according to either

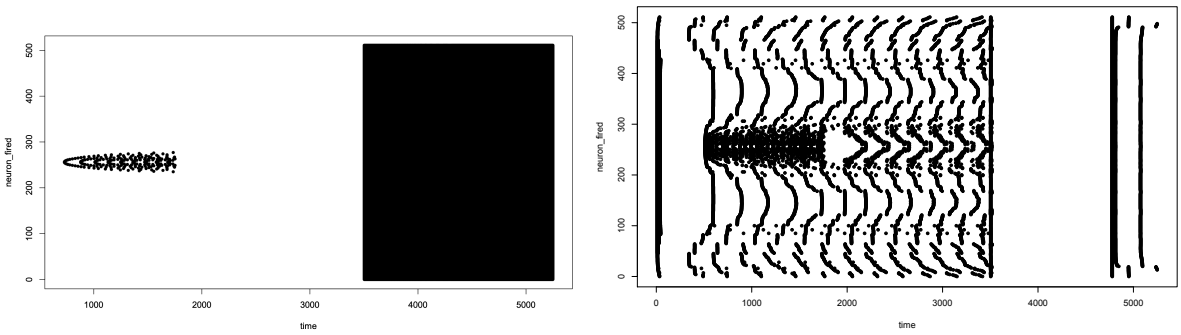

(a) I_{syn} (equation 1.2) (b) I^*_{syn} (equation 3.4)

Figure 4.4: Simulations of networks with two different definitions of the synaptic current. Stimulation angle $\theta_{stim} = 180°$. (a) Network with synaptic current computed according to equation 1.2 shows no significant spiking activity in the delay period, and massive spiking activity on the response period. This is opposite to (b), where rich bursting activity can be noticed in the delay period, and no activity in the response period. When the stimulation angle θ_{stim} is 180°, the maximum stimulation is given to the neuron with index $i = 256$.

synaptic current definition	**input sign control**	**label distribution**	**parameter set**	e	α	μ	θ_{stim}
inverse	no	uniform	control	-2	30	29	180°

Table 4.1: Parameters of the network used in the 'reference' simulation.

equation 1.2 or equation 3.4, while all the other parameters remained the same. These two networks are shown in figure 4.4. A network which utilized the inverse definition of the synaptic current I^*_{syn} (figure 4.4b) showed richer activity centered around the stimulation angle and switched off during the response period and subsequently went to the pre-stimulation state. Other network properties and parameters are shown in table 4.1.

Synaptic input sign control (see section 3.2) was used in a similar simulation with the inverse synaptic input definition (figure 4.5). Neuronal activity during the delay response period was more homogeneous and the activity around the stimulation angle θ_{stim} was weaker than in the no-sign-control condition with the inverse synaptic input.

In the following text, the network with the inverse definition of the synaptic current and with no sign control shown in figure 4.4b functions as the reference, and we present only simulations where some of the parameters were changed compared to simulation in figure 4.4b. Parameters of this network are displayed in table 4.1.

This *reference* simulation showed a clear neuronal firing desynchronization pattern around the stimulation cue, which took a form of a series of *waves* oriented to the

right, in the temporal direction of the simulation. Pyramidal cells showed higher synchronization in neighboring areas.

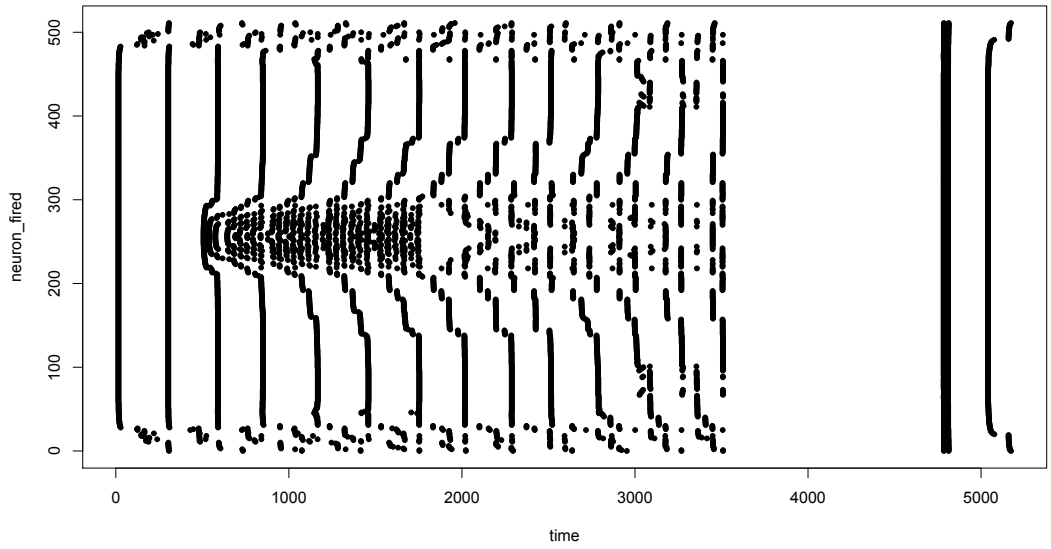

Figure 4.5: Rastergram of a simulation with the synaptic input sign control. Cue presented at $\theta_{stim} = 180°$.

4.3.2 Channel conductance and strength connections

We looked for an appropriate level of the network connectivity by manipulating the exponent e while retaining the base of the channel conductance parameter values as assigned in the control parameter set. In the simulations, no neuronal activity was present in the delay period for $e \leq -2.6$ and we concluded that the network displayed too much activity when $e \geq -1.6$. Figure 4.6 shows the network's behavior when different values of e, $-2.6 \leq e < -1.6$, were employed.

We also decreased or increased the strength of the isodirectional connections J^{+}_{EE} ($1.4 \leq J^{+}_{EE} \leq 1.8$). However, we did not notice any significant change in the firing pattern.

4.3.3 Choosing the better neuronal label distribution

Simulations with no selective transient current injected during the cue presentation period showed different patterns of spontaneous neuronal activity. Uniform distribution of neuronal labels behaved in a calmer manner (see figures 4.7a and 4.7b), while non-uniform distribution showed richer and more varied activity patterns in some of the regions (see figures 4.7c and 4.7d). Both distributions showed lateral symmetry, as it can be seen in figure 4.7.

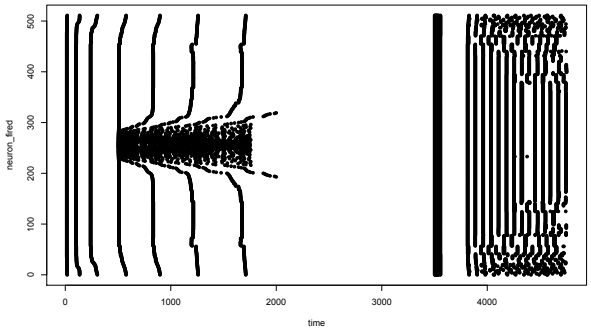

(a) $e = -2.6$

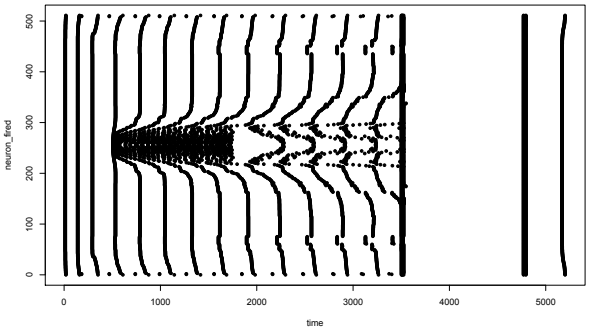

(b) $e = -2.4$

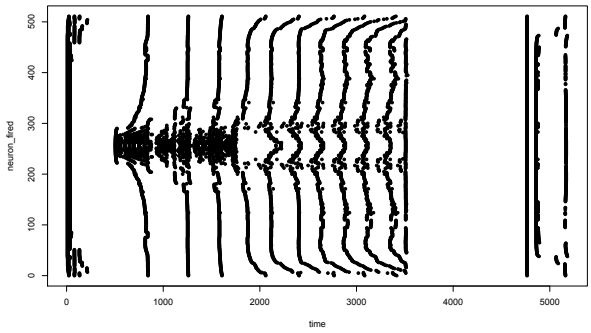

(c) $e = -1.8$

Figure 4.6: Networks with different levels of channel conductances. It can be seen that greater values of the exponent e enhance the width of the center of elevated neuronal activity and more activity is spread out to the neighboring regions with greater values of e. The conductances in (a) are too small and the activity does not persist during the delay period. On the other hand, stimulation of the whole network during the response period gives rise to high spiking activity towards the end of the simulation. In this figure, (a) $e = -2.6$, (b) $e = -2.4$ and (c) $e = -1.8$.

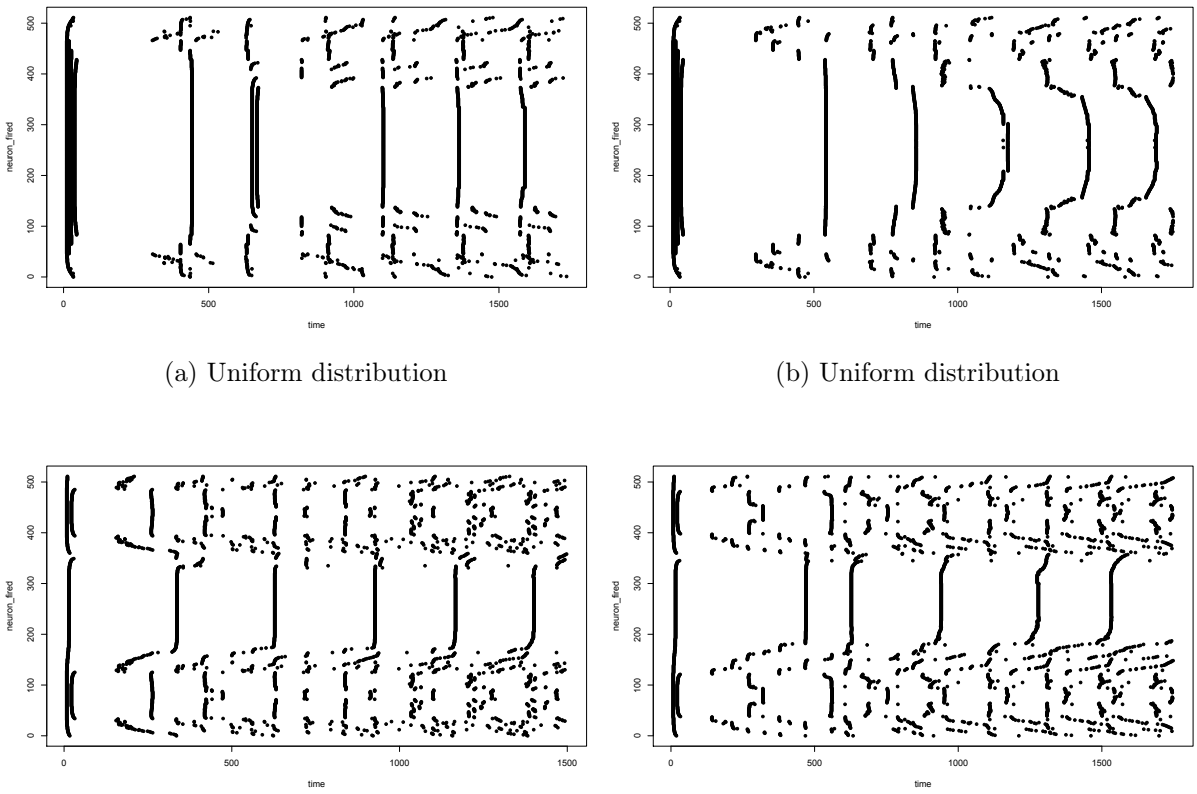

(a) Uniform distribution

(b) Uniform distribution

(c) Non-uniform distribution

(d) Non-uniform distribution

Figure 4.7: Rastergram of spontaneous firing activity of unstimulated network. Subfigures (a) and (b) show spontaneous activity of a network whose neurons are uniformly labeled, whereas neurons in the networks shown in subfigures (c) and (d) are non-uniformly labeled.

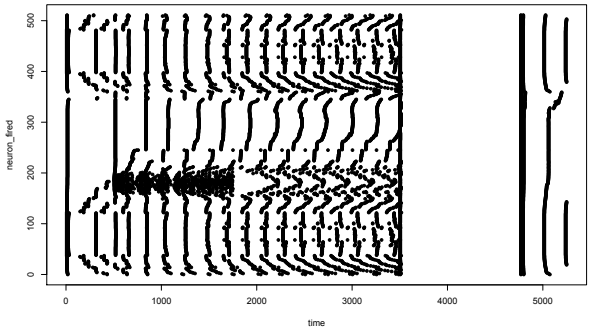

(a) $\theta_{stim} = 180°$

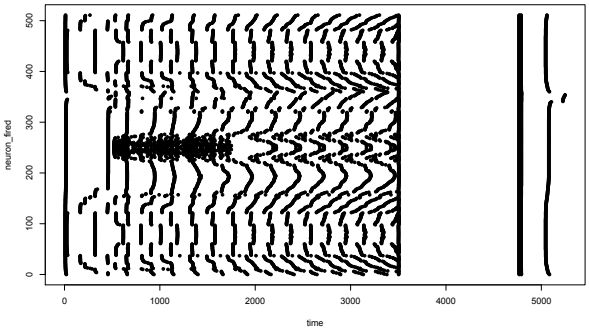

(b) $\theta_{stim} = 250°$

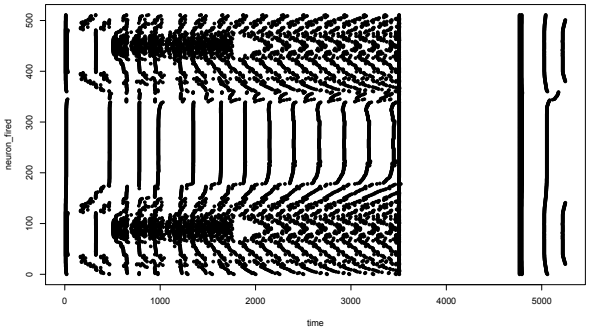

(c) $\theta_{stim} = 90°$

Figure 4.8: Activity of a network with non-uniform neuronal distribution. The figure shows three stimulation angles: (a) 180°, (b) 250°, (c) 90°.

We simulated the network with no stimulation to see how the stimulation affected the network's activity when the non-uniform distribution was used. Next simulations were done with the same network properties as shown in table 4.1 except for using the non-uniform distribution. Figure 4.8 shows how the network behaved under different stimulation angles. The 90° cue (figure 4.8c) showed significantly stronger activity in the stimulated region compared to 180° and 250° (figure 4.8a, 4.8b). This activity was supposedly due to the slightly higher number of neurons with preferred cue angle close to 90° (see section 3.2).

4.3.4 Effects of different stimulation input current strength

When different input current strengths α were used, different activity patterns emerged in the region close to the stimulus angle. Simulations with different values of α (5, 7.5, 10, 20 and 50) can be seen in figure 4.9. Stimulation current amplitude during the response period was 4α.

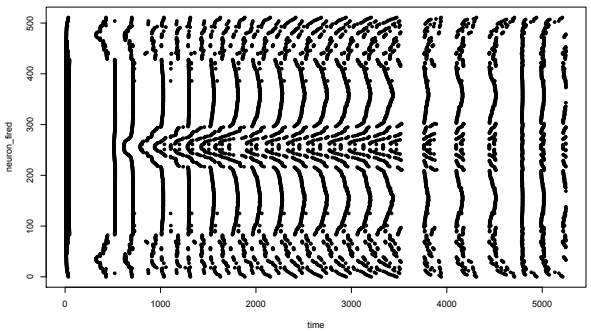

(a) $\alpha = 5$

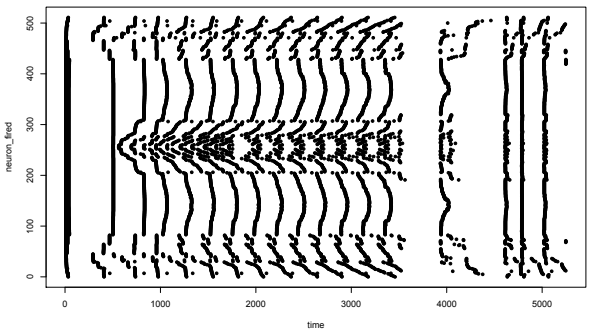

(b) $\alpha = 7.5$

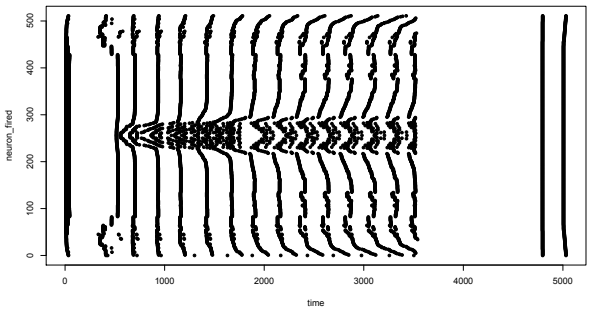

(c) $\alpha = 10$

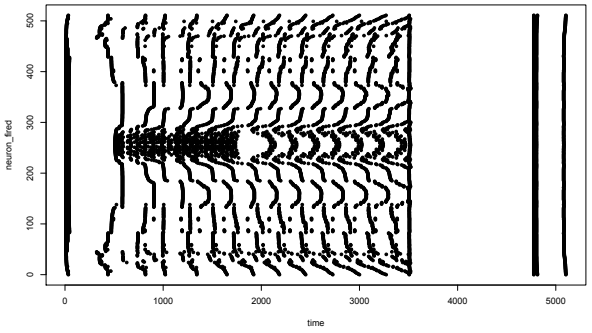

(d) $\alpha = 20$

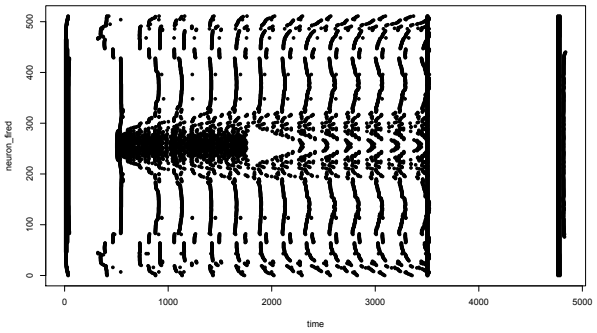

(e) $\alpha = 50$

Figure 4.9: Rastergram of the network stimulated with different values of the peak current: (a) $\alpha = 5$, (b) $\alpha = 7.5$, (c) $\alpha = 10$, (d) $\alpha = 20$, (e) $\alpha = 50$.

4.3.5 Longer simulation

We performed a simulation where the pre-trial and the post-trial periods were 200 ms long, the cue presentation and the response period were 250 ms long and the delay period was 2500 ms long. This was the longest simulation performed in this series of simulations. Parameter set used was the same as shown in table 4.1. It showed an activity pattern similar to the simulation figure 4.4b. In later stages of the delay period, desynchronization patterns emerged also in other regions of the network. We measured the spiking frequency of pyramidal cells during the delay period. It showed areas of higher and lower spiking frequency, however all the frequencies were in 18 - 24 Hz frequency band. Figure 4.10 shows rastergram and spiking frequency of neurons in the network.

4.4 Activity of interneurons

Simulation of the network shown in figure 4.4b, in which only pyramid-to-pyramid connections were spatially tuned, showed strong spiking activity of interneurons in the pre-trial period, bursts of spikes followed by calmer activity during the cue presentation period, which was being stabilized towards the delay period. Regular and stable activity in the delay period was followed by selective activity in some of the regions during the response period and a quite homogeneous spiking activity during the post-trial period. This activity can be shown in figure 4.11a.

Simulation figure 4.11c was performed with spatial tuning of pyramid-to-interneuron connections. The values of relevant parameters were set according to Compte and his colleagues [6] and were $J_{EI}^{+} = 1.25$ and $\sigma_{EI} = 18°$. Other parameters were set according to table 4.1.

Figures 4.11b and 4.11d show spiking frequencies of interneurons in these simulations. Interneurons in the simulation with no spatial tuning of pyramid-to-interneuron connections were in a slightly lower and narrower frequency band of 112 - 116 Hz and their spiking frequencies were more uniformly distributed than in the simulation with spatial tuning of pyramid-to-interneuron connections. We can see how the spatial tuning affected the interneurons. Regions with higher frequency rate are towards the middle of the scatterplot. These are the regions with preferred cues closer to the stimulated cue angle. Similar distribution of firing rates can be found with pyramidal cells in different simulation shown in figure 4.10. The frequency band was 105 - 130 Hz.

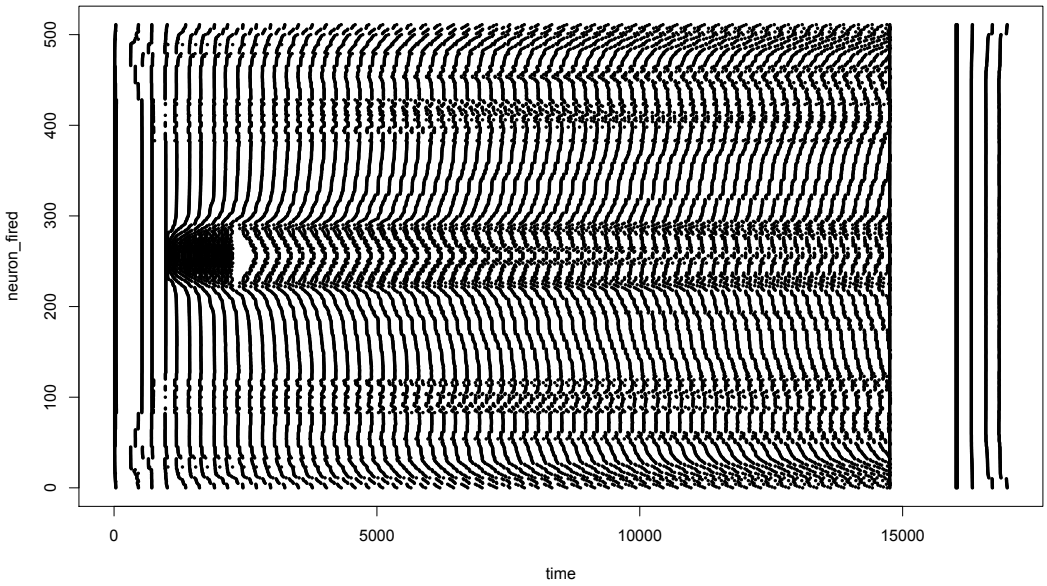

(a) Rastergram of the activity of the pyramidal cells

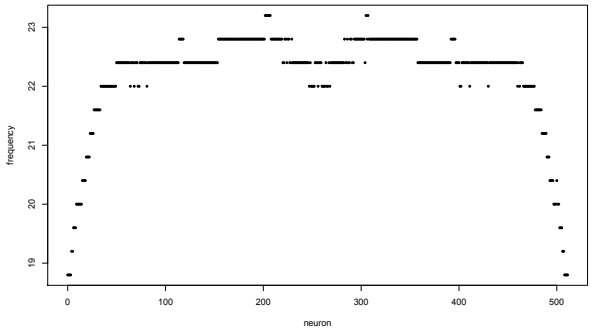

(b) Frequency of firings of the pyramidal cells during the delay period

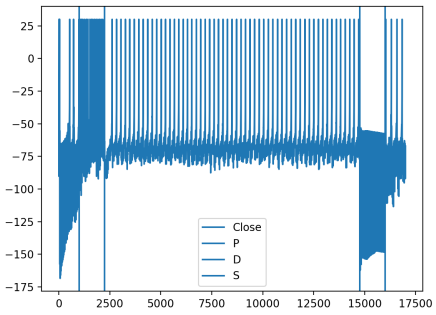

(c) Membrane potential time development of a neuron close to the presented cue angle

Figure 4.10: Simulation with a 2500 ms long delay period shows in (a) a slow decay of the desynchronization pattern around the stimulation angle $\theta_{stim} = 180°$ and emergence of desynchronization patterns in the regions farther from the stimulated cue angle θ_{stim} as the delay period progressed. In the after-trial period, following the response period, the neurons fire rather synchronously. (b) Higher spiking frequency is located in regions closer to the presented cue angle. (c) Time development of the membrane potential v of a neuron close to the presented cue angle shows rather irregular activity at the beginning of the experiment, very high spiking activity during the presentation period, rather regular spiking activity of a frequency lower than in the cue presentation period during the delay period, low level activity with no spikes during the response period, and a periodic spiking activity during the post-trial period.

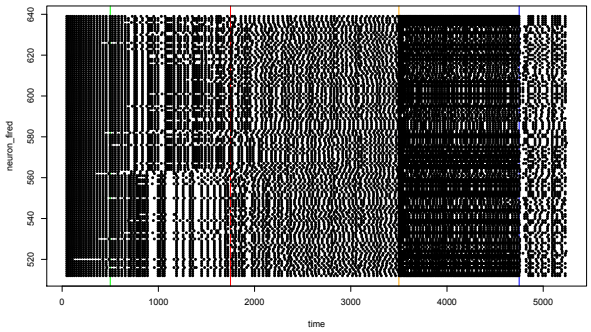

(a) No p-to-i spatial tuning - rastergram

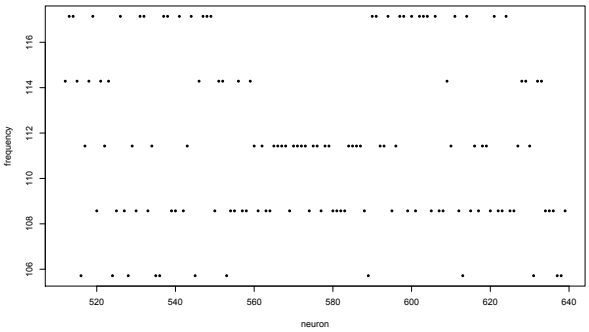

(b) No p-to-i spatial tuning - frequency

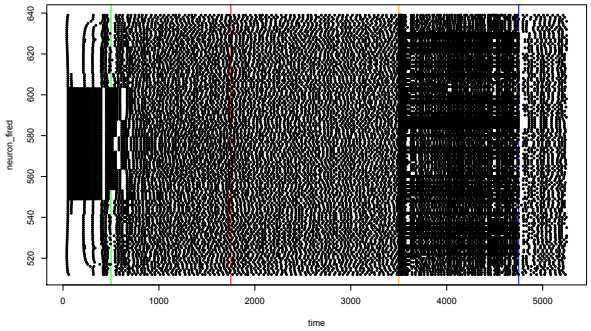

(c) P-to-i spatial tuning - rastergram

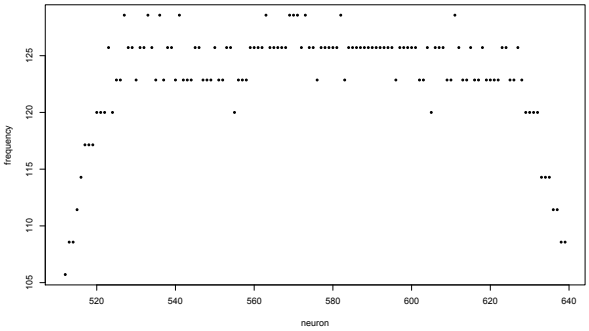

(d) P-to-i spatial tuning - frequency

Figure 4.11: Activity of interneurons in a simulation with and without spatial tuning of pyramid-to-interneuron connections. (a) and (b) show rastergram and spiking frequencies of interneurons without spatial tuning of pyramid-to-interneuron connections, (c) and (d) show rastergram and spiking frequencies of interneurons with spatial tuning of pyramid-to-interneuron connections. For the sake of clarity, green line marks the beginning of the cue presentation period, red of the delay period, orange of the response period and blue of the post-trial period in these rastergrams.

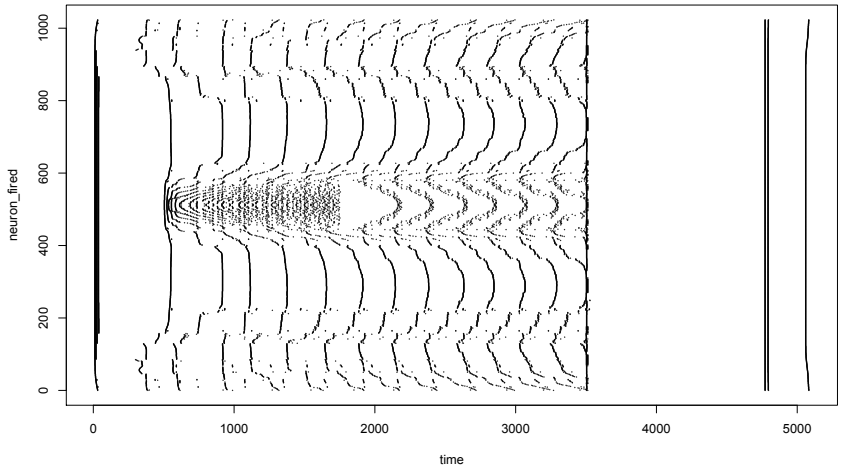

Figure 4.12: Simulation of a network with 1024 excitatory and 256 inhibitory neurons.

4.5 Simulation of a larger network

We also simulated a network two times smaller than the network used by Compte and his colleagues [6]. It was simulated with the control parameter set multiplied by 2×10^{-2}. The other parameters used in this simulation were the same as displayed in table 4.1. This network displayed elevated activity pattern similar to the reference network. This simulation can be seen in figure 4.12.

4.6 Simulations with distractors

With distractors, we looked at how different distances between the stimulation angle θ_{stim} and the distraction angle θ_d affect the distraction. Stimulation angle $\theta_{stim} = 180°$ and two different distraction angles were chosen: $\theta_{d,1} = 230°$ and $\theta_{d,2} = 300°$. Two different selective transient input current values $\alpha_1 = 20$ and $\alpha_2 = 10$ were tested to see how the network is distracted when different stimulation strength is imposed. The network used was four times smaller than in Compte et al. [6]. Neurons were uniformly labeled with their preferred cue angle (see section 3.2). Other parameters were similar to the 'reference' network shown in figure 4.4b. The onset of the original stimulus was at 100 ms and lasted for 250 ms. The onset of the distractor stimulus was at 200 ms after the beginning of the delay period and lasted for another 250 ms.

Figures 4.13a and 4.13c show that two traces which emerged during the stimulations at two particular angles and two different times moved towards each other when they were close to each other.

In simulations in which the two angles were separated by more than 90°, the two traces remained more or less the same throughout the whole delay period. Distrac-

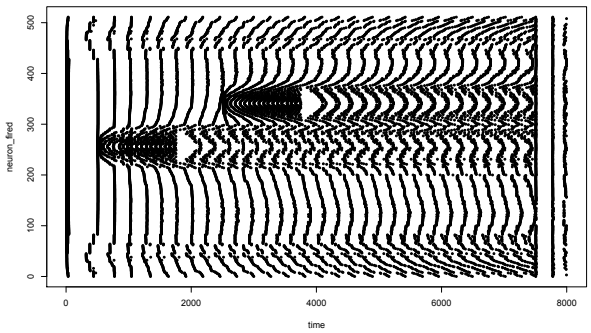

(a) $\theta_d = 230°$, $\alpha = 20$

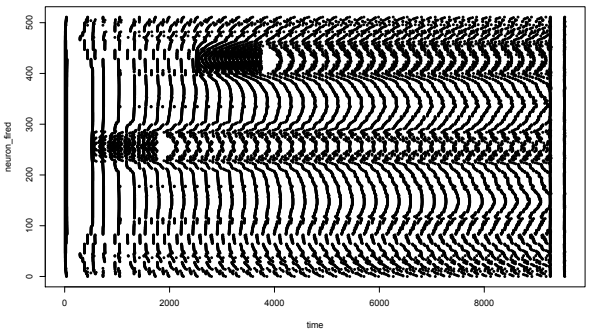

(b) $\theta_d = 300°$, $\alpha = 20$

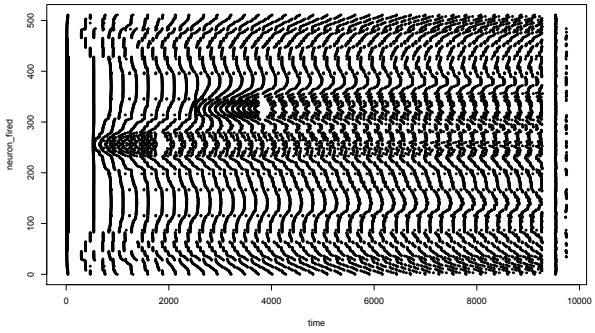

(c) $\theta_d = 230°$, $\alpha = 10$

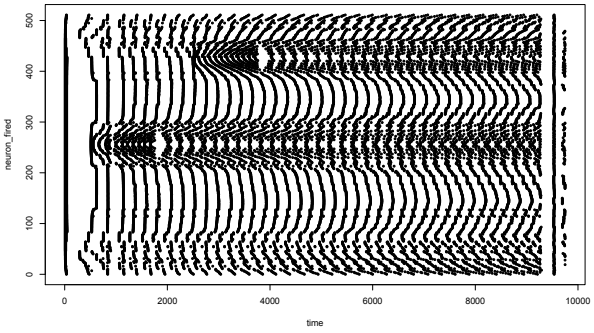

(d) $\theta_d = 300°$, $\alpha = 10$

Figure 4.13: Simulations in which distractors were introduced 200 ms after the beginning of the delay period. In (a) and (c), cue period stimulation angle θ_{stim} and distraction angle θ_d are close to each other ($|\theta_{stim} - \theta_d| < 90°$). In (b) and (d), $|\theta_{stim} - \theta_d| > 90°$. Simulations (a) and (b) were done with a higher stimulation peak strength than simulations (c) and (d).

tion caused some changes in the activity pattern of the traces originating in the cue presentation. These changes were, however, not very prominent.

4.7 Simulations of other parameter sets

Here we present simulations done either with the modulated parameter set [6] or the parameter set used by Almeida and her colleagues [1]. Parameters of these sets can be found in table 1.1.

The modulated parameter set showed behavior similar to the control parameter set. However, the pattern around the stimulation angle was less prominent and the activity in other regions was richer and more desynchronized, as shown in figure 4.14a.

The parameter set used by Almeida and her colleagues [1] showed a significant amount of activity in all regions during the cue presentation and the delay periods. The

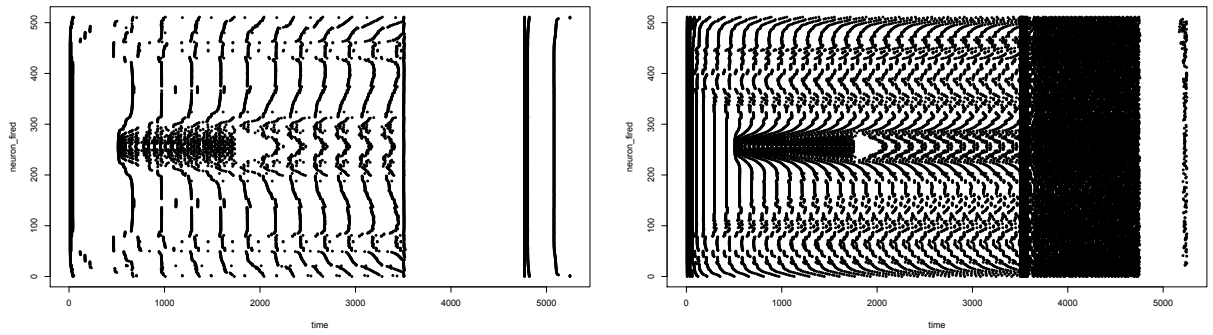

(a) Modulated parameter set [6] (b) Parameter set from Almeida et al. [1]

Figure 4.14: Pyramidal cell firings when two different parameter sets used: (a) modulated parameter set [6], (b) parameter set used by Almeida and her colleagues [1].

exponent e had to be radically lowered. Although, this problem might have occurred only because time step of 0.2 ms was used in this simulations. Also, all pyramidal cells showed high firing activity during the presentation of the stimulus to the whole network during the delay period. This activity switched off only after the disappearance of the stimulus. Figure 4.14b shows a rastergram of a simulation with the Almeida et al. [1] parameter set with the exponent e lowered to the value -2.8.

4.8 Simulation using 0.02 ms time step

In the following simulation, we used time step 0.02 ms, which was used by Compte et al. [6]. Parameters used are as shown in table 4.1 with one exception: the exponent e was set to -1. Lengths of periods were as presented in section 4.3. Figure 4.15a shows the simulation until the beginning of the response period. Pyramidal cells exhibited activity patterns similar to those found in the simulation figure 4.4b. Higher frequency of firing activity in regions closer to the stimulated cue angle can be seen in figure 4.15b. Frequency band was 20 - 35 Hz.

When e was set to -2, no delay period activity was present, suggesting that this order of magnitude did not lead to sufficiently strong connections when the time step of 0.02 ms was used. The exponent e set to 0 led to too strong neural activity of the network.

This simulation showed that the network simulated with a smaller time step displayed similar behavior to the network simulated with a greater time step when the synaptic conductance variables were increased to a sufficiently high level.

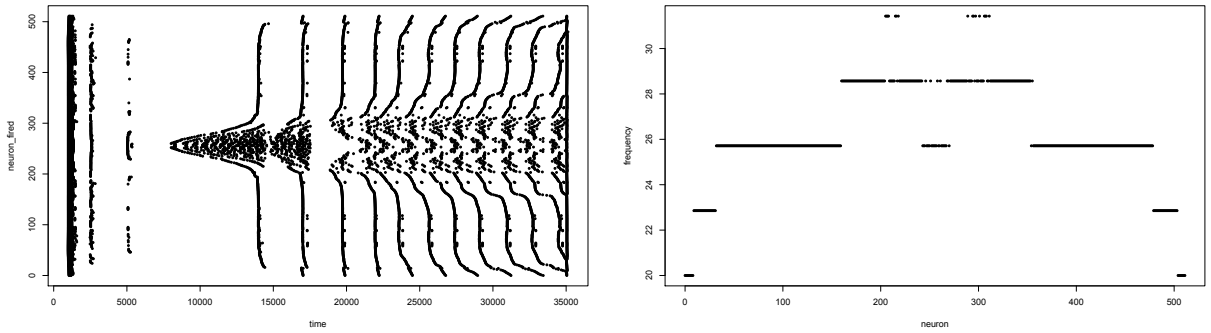

(a) Rastergram of the simulation

(b) Frequencies of neuronal firings

Figure 4.15: Simulation of a network which uses 0.02 ms time step. (a) Rastergram of neuronal activity during the pre-trial, the cue presentation and the delay periods, (b) firing frequencies of pyramidal neurons during the delay period.

Chapter 5

Overall results of the simulations

In this section, we present the overall results of our simulations. For a detailed description of individual simulations, see chapter 4.

5.1 Emergence of the elevated activity

The network we implemented managed to build up an elevated activity in the stimulated subpopulation of pyramidal cells during the cue presentation period. This subpopulation of neurons remained active when the stimulus vanished. However, frequency of firings of each individual neuron in the subpopulation was relatively lower during the delay period compared to the cue presentation period. The network displayed stronger desynchronization in the region close to the stimulus cue angle than in other regions. Most simulations (see section 4.3) suggest that the whole network was affected by the stimulation, and not only a selected area of pyramidal cells.

Similar patterns of activity were found when different number of neurons was used in the network (section 4.5), other parameter sets were used (section 4.7) or a different time step was used (section 4.8).

5.2 The network switches off

The simulations presented in section 4.3 showed that the network was able to switch off. Supposedly due to the activity of interneurons, the network displayed significant decrease of activity of pyramidal cells during the response period and no selective elevated firing activity in the region close to the stimulation angle in the subsequent post-trial period.

5.3 Time step and network connectivity

We state that the selected time step had an enormous impact on the accuracy of the behavior of the network. A sufficiently small time step had to be used in order to achieve the right amount of the network's activity and to use sufficiently strong connection between the neurons. Simulations in section 4.1 used time step 1 ms. Although elevated spiking activity of stimulated neurons persisting during the delay period was built when 1 ms time step was used, the connections were presumably not strong enough to make the network switch off. The order of magnitude of the channel conductance variables was -3 (we used the variables as dimensionless). When the same order of magnitude was used with 0.2 ms time step, no persistent elevated selective spiking activity developed. It was necessary to increase the channel conductances to -2 order of magnitude (for comparison, see figures and 4.4b and 4.6). A simulation performed with time step 0.02 ms (see section 4.8) showed a similar activity pattern than simulations performed with time step 0.02 ms when the order of magnitude of the channel conductance variables was -1. This network did not exhibit any firing behavior of the pyramidal cells with the order of magnitude -2. It is, thus, clear that the level of neuronal connectivity in our implementation of the model [5] is very sensitive to the time step used.

5.4 Two definitions of the synaptic current

In Compte et al. [6], the synaptic current is computed as defined by equation 1.2. In this equation, the synaptic reversal potential V_{syn} is subtracted from the presynaptic membrane potential v. Such a definition is also used in several other studies employing the Simple model of spiking neurons [14] (e.g. Izhikevich [16] and Wacongne et al. [25]). However, Izhikevich [17] also defined the synaptic current similarly to equation 3.4 (the inverse definition), i.e. the presynaptic membrane potential v is subtracted from the synaptic reversal potential V_{syn}. We tested both definitions of the synaptic current in our simulations. Our implementation of the model showed satisfying results only when the inverse definition was employed, as it can be seen in figure 4.4.

5.5 Assigning preferred cue angles

We found and tested two methods of labelling the neurons with preferred cue angles, called uniform and non-uniform (described in section 3.2). The non-uniform distribution, unlike the uniform distribution, enhanced neuronal activity in some regions. It was so because there were more neurons with the same preferred cue angle than in other regions. Therefore, uniform distribution gave more satisfactory results.

5.6 Stimulation strength

Different transient current stimulation peak amplitudes α resulted in different enhanced activity patterns in the neuronal regions with preferred cue angle close to the stimulation angle. However, all tested current amplitudes α resulted in the selective enhanced activity. Overview of different strengths can be seen in figure 4.9. We used $\alpha = 30$ in most simulations and amplitude of the transient current injected to all neurons during the response period was set to 4α in order to give the neurons strong enough stimulation to overcome the 'bump' state and reset the neuronal activity.

5.7 Network size

Simulation of a larger network of 1024 pyramidal cells and 256 interneurons (figure 4.12) showed similar after-stimulation pattern than simulations with 512 pyramidal cells and 128 interneurons.

5.8 Distractors

Simulations with distractors showed different behavior when the cue presentation angle θ_{stim} and the distractor angle θ_d are separated by an angle smaller or larger than 90°. We could clearly see how this two traces approached each other. With separation angle greater than 90°, the two traces remained more-less unaffected.

Chapter 6

Discussion

Regarding the practical part of our thesis - the implementation of the spatial working memory model [1, 6, 7] employing the Simple model of spiking neurons [14], we have managed to develop a computer program following the description of the spatial working memory model by Compte and his colleagues [6], using some elements of the model described by Edin and the collective of co-authors [7] or Almeida and her colleagues [1], and the description of the Simple model of spiking neurons [14, 17]. We have run hundreds of simulations in order to learn how the model works when the Simple model of spiking neurons is used, tune the parameters of the model to get plausible results and see how maniputating these parameters changes the properties of the implemented network. Several of these simulations are presented in chapter 4.

In this chapter, we evaluate our implementation, compare our results to the results of Compte et al. [6], describe issues and limitations we encountered and frame our work in a larger scope of theoretical research in this field.

6.1 Evaluation

We identified two main features of the model of the spatial working memory [6]. One of them was its ability to develop selective elevated neuronal activity in a stimulated subpopulation of pyramidal neurons which persisted also after disappearance of the stimulus (so called 'bump state'). The second one was the ability of the network to override this persistent selective enhanced activity when all the neurons were stimulated (see sections 1.2.3 and 2).

Our findings suggest that this behavior can be accomplished when the network is implemented using the Simple model of spiking neurons [14]. However, we did not directly detect elevated activity in the region close to the stimulated angle in a way it was shown in simulations of Compte and his colleagues [6] (see figure 1.5). The stimulus-induced selective delay period activity was rather manifested as a distinctive

and prominent desynchronization pattern (see section 4.3) and we concluded that the behavior of the whole network was influenced by the stimulation. This desynchronization means that the neurons in the stimulated area showed larger differences in their spiking times. However, each neuron spiked at relatively precise timings, with its unique frequency (e.g. shown in figure 4.10c).

Also, our network generally behaved in a more synchronous manner and neurons very often fired one after each other, forming different patterns of activity.

In our simulations, the network very clearly switched off when all the neurons were stimulated in the response period. What followed, was an activity pattern similar to the one exhibited by the neurons before the cue presentation period.

In simulations with distractors, we showed attraction when the presented cue angle and the distractor angle were separated by an angle smaller than 90°.

We tried different network sizes, time steps and simulation lengths. Our simulations with a larger network, a larger simulation length, or a smaller time step showed similar behavior than simulations of a shorter length, a smaller time step, or a smaller network. There was, however, one exception: the simulations done with 1 ms time step did not show a very accurate behavior (see section 4.1). We concluded that this was largely due to the limitations imposed by this time step on the possible connectivity level.

6.2 Issues and limitations

Largely due to technical reasons, in most of our simulations, we used a network four times smaller than the network originally used [6]. Also the time step we used in most simulations was 10 times larger than originally. It was clear that the time step used related directly to the possible strengths of the connection in the network and, thus, had impact on the behavior of the network. Smaller time step allowed for stronger connections. Also smaller time step increased the network's accuracy.

From the software development perspective, it took quite a long time to compute a relatively short simulation 700 ms at 0.2 ms time step. This was partially caused by the hardware used.

Regarding theoretical limitations, according to Compte [5], computational models such as the one we implemented did not completely show a biologically plausible behavior (for comparison, see section 1.2.5). They did not account for some features exhibited by biological neurons during the oculomotor delayed-response task experiments [10] (see section 1.1.1.

6.3 Interdisciplinarity

Our thesis is mostly embraced by the field of computational cognitive neuroscience. It employs parts of computer science, software development and computational modelling to study a topic related to cognitive psychology. Using tools of computer science to study and understand cognitive phenomena more thoroughly is a standard research trend in cognitive science [21].

6.4 Significance

In our thesis, we implemented and tested an existing model of the spatial working memory proposed originally by Compte and his colleagues [6] using a different model of neurons. Originally, leaky integrate-and-fire units were used [22, 15], but we implemented it using the Simple model of spiking neurons [14], which is more powerful in simulating behavior of various types of neurons than the former model. Yet, we did not find any study in which the spatial working memory model [6] was implemented using the Simple model of spiking neurons [14]. Therefore, our thesis might be the first step towards using the spatial working memory model [6] together with the Simple model of spiking neurons [14] in a research, thus integrating this model of the spatial working memory [6] into the part of the brain research using the Simple model of spiking neurons [14].

6.5 Future work

First of all, further investigation on how the network would behave if the number of neurons was set to the number originally used by Compte and the collective [6] is needed. It might be also beneficial if larger networks than that would be simulated.

In all of our simulations, we based the parameters on either control parameter set, modified parameter set [6], or a parameter set used in Almeida et al. [1]. Only some of the parameters were manipulated to see how their modifications change the network's behavior. However, we propose to further investigate how a finer parameter tuning may affect the network's behavior.

$AMPA$-mediated synaptic channels were omitted from the implemented network. It was done so because $AMPAR$ channels were not used in most of the simulations of Compte et al. [6], either. However, some simulations in the paper by Compte and his colleagues [6] also employed $AMPAR$ channels. Therefore, the next step might be to include them in some of the simulations with the Simple model of spiking neurons [14].

We should also take the time which it took to run our simulations. If we keep in mind that Compte and his colleagues [6] run their simulations at a *Pentium III*

processor and a simulation of a few seconds with a network 4 times bigger than the network we used took them approx. 2.5 hours to run, we have to say that the code and compiling process has to be optimised. Compte and his colleagues [6] used the programming language *C++*, whereas we used *Python 2*. Therefore, it also might be beneficial to program our implementation of the model in faster *C++*.

Moreover, we concluded that the synaptic current as defined by equation 3.4 must be used when the Simple model of spiking neurons is employed [14]. This follows the suggestion by Izhikevich [17], but it contradicts how the synaptic current was computed in most of the related research [1, 6, 7, 16, 25]. It might be needed to research why the synaptic current as defined by equation 1.2 does not lead to plausible results, although we proposed some intuition behind this (see section 4.1).

We showed prominent desynchronization patterns in the delay period, following the selective stimulation during the cue presentation period. However, mechanisms beyond these patterns have to be, yet, researched.

Last but not least, replication of existing research related to the topic [1, 7] using the Simple model of spiking neurons [14] would be beneficial to figure out how using the model of the spatial working memory [6] would be in accordance with the state of the art in the field of the spatial working memory research.

Conclusion

The aim of this Master's thesis was to implement the model of spatial working memory [1, 6, 7] employing the Simple model of spiking neurons [14].

In the theoretical part of this thesis (chapter 1), we analysed the theoretical background of our thesis: the spatial working memory and a theoretical model of its underlying cellular mechanisms as proposed by Goldman-Rakic [12], the model of spatial working memory [1, 6, 7] and the Simple model of spiking neurons [14].

Using the information presented in chapter 1, we implemented the model of spatial working memory using the Simple model of spiking neurons. The model of spatial working memory was originally implemented employing the leaky integrate-and-fire neurons [22], which according to Izhikevich [14] could not produce rich spiking and bursting behavior patterns of cortical neurons and, therefore, its ability to simulate the brain functions was limited. On the other hand, the Simple model of spiking neurons was capable of producing behavior of majority of cortical neurons in the human brain [14, 15, 17]. Therefore, we implemented the model of the spatial working memory using this neuron model [14], in hope that it can be better integrated to models of large brain structures, like the prefrontal cortex.

We tested our implementation of the model [6] by simulating the oculomotor delayed-response task [10], looking for its main feature: the ability to build a selective elevated activity when a subpopulation of excitatory neurons is stimulated. This elevated activity persists when the stimulation ends (delay period) and vanishes when the whole network is stimulated (response period). We manipulated several parameters of the model to find a plausible result and study how manipulating this parameters affects the network's behavior. We used several proposed types of the model [1, 6, 7] and tested how the network behaves when distracted by different stimuli in the delay period of the oculomotor delayed-response task [10].

We found out that this selective elevated activity was manifested as patterns of frequent spikes of pyramidal neurons in the region in which neurons' preferred cue angles were close to the presented cue angle. It was characterized by a sequence of neuronal firings with a lot of phase shifts between different neurons in the region. Other regions in the network showed more synchronous activity.

Nature of these activity patterns that emerged in our simulations has not yet been

studied. Therefore, it is needed to perform theoretical and practical research to study these patterns in more detail.

Our thesis showed that the model of the spatial working memory [1, 6, 7] can be implemented and the oculomotor delayed-response task [10] can be simulated using the Simple model of spiking neurons. However, the results are partly different from the results of previous computational studies (e.g. [1, 6, 7]). These differences are mainly in the microstructure of neuronal firings.

Our results can contribute to the simple spiking neurons related research and help in integration of the spatial working memory model [6] to the part of computational neuroscientific research employing the Simple model of spiking neurons [14].

Bibliography

[1] Rita Almeida, João Barbosa, and Albert Compte. Neural circuit basis of visuospatial working memory precision: a computational and behavioral study. *Journal of neurophysiology*, 114(3):1806–1818, 2015.

[2] Alan David Baddeley. Working memory. *Philosophical Transactions of the Royal Society of London. B, Biological Sciences*, 302(1110):311–324, 1983.

[3] Nicolas Brunel and Xiao-Jing Wang. Effects of neuromodulation in a cortical network model of object working memory dominated by recurrent inhibition. *Journal of computational neuroscience*, 11(1):63–85, 2001.

[4] Thomas B Christophel, P Christiaan Klink, Bernhard Spitzer, Pieter R Roelfsema, and John-Dylan Haynes. The distributed nature of working memory. *Trends in cognitive sciences*, 21(2):111–124, 2017.

[5] Albert Compte. Computational and in vitro studies of persistent activity: edging towards cellular and synaptic mechanisms of working memory. *Neuroscience*, 139(1):135–151, 2006.

[6] Albert Compte, Nicolas Brunel, Patricia S Goldman-Rakic, and Xiao-Jing Wang. Synaptic mechanisms and network dynamics underlying spatial working memory in a cortical network model. *Cerebral cortex*, 10(9):910–923, 2000.

[7] Fredrik Edin, Torkel Klingberg, Pär Johansson, Fiona McNab, Jesper Tegnér, and Albert Compte. Mechanism for top-down control of working memory capacity. *Proceedings of the National Academy of Sciences*, 106(16):6802–6807, 2009.

[8] GN Elston. Evolution of nervous systems. 2007.

[9] T. Freund and S. Kali. Interneurons. *Scholarpedia*, 3(9):4720, 2008. revision #89023.

[10] Shintaro Funahashi, Charles J Bruce, and Patricia S Goldman-Rakic. Mnemonic coding of visual space in the monkey's dorsolateral prefrontal cortex. *Journal of neurophysiology*, 61(2):331–349, 1989.

[11] Wulfram Gerstner, Werner M Kistler, Richard Naud, and Liam Paninski. *Neuronal dynamics: From single neurons to networks and models of cognition*. Cambridge University Press, 2014.

[12] Patricia S Goldman-Rakic. Cellular basis of working memory. *Neuron*, 14(3):477–485, 1995.

[13] Plotly Technologies Inc. Collaborative data science. `https://plot.ly`, 2015.

[14] Eugene M Izhikevich. Simple model of spiking neurons. *IEEE Transactions on neural networks*, 14(6):1569–1572, 2003.

[15] Eugene M Izhikevich. Which model to use for cortical spiking neurons? *IEEE transactions on neural networks*, 15(5):1063–1070, 2004.

[16] Eugene M Izhikevich, Joseph A Gally, and Gerald M Edelman. Spike-timing dynamics of neuronal groups. *Cerebral cortex*, 14(8):933–944, 2004.

[17] Eugene M Izhikevich and Jeff Moehlis. Dynamical Systems in Neuroscience: The geometry of excitability and bursting. *SIAM review*, 50(2):397, 2008.

[18] R Core Team. *R: A Language and Environment for Statistical Computing*. R Foundation for Statistical Computing, Vienna, Austria, 2017.

[19] Srinivas G Rao, Graham V Williams, and Patricia S Goldman-Rakic. Isodirectional tuning of adjacent interneurons and pyramidal cells during working memory: evidence for microcolumnar organization in PFC. *Journal of neurophysiology*, 81(4):1903–1916, 1999.

[20] Botond Szatmáry and Eugene M Izhikevich. Spike-timing theory of working memory. *PLoS Comput Biol*, 6(8):e1000879, 2010.

[21] Paul Thagard. Being interdisciplinary: Trading zones in cognitive science. *Interdisciplinary collaboration: An emerging cognitive science*, pages 317–339, 2005.

[22] Henry C Tuckwell. Introduction to theoretical neurobiology. Cambridge Cambridgeshire, 1988.

[23] Guido Van Rossum and Fred L Drake Jr. *Python reference manual*. Centrum voor Wiskunde en Informatica Amsterdam, 1995.

[24] Van Rossum, Guido and Drake, Fred L. *Python 3 Reference Manual*. CreateSpace, Scotts Valley, CA, 2009.

[25] Catherine Wacongne, Jean-Pierre Changeux, and Stanislas Dehaene. A neuronal model of predictive coding accounting for the mismatch negativity. *Journal of Neuroscience*, 32(11):3665–3678, 2012.

[26] Xiao-Jing Wang. Synaptic basis of cortical persistent activity: the importance of NMDA receptors to working memory. *Journal of Neuroscience*, 19(21):9587–9603, 1999.

[27] Eric W Weisstein. Erf. `https://mathworld.wolfram.com/`, 2002.

[28] Eric W Weisstein. Euler Forward Method. `https://mathworld.wolfram.com/`, 2016.

Appendix A - Electronic attachment

Source codes of our implementation are included together with a short instruction file *README.txt* on a CD attached to this thesis. We include code of simulations with and without distractors. This CD also contains vizualizations of results of our simulations displayed in chapter 4. Contents of this CD can be found in the *CONTENTS.txt*.